

Geometric interpretation of the multi-scale entanglement renormalization ansatz

Ashley Milsted¹ and Guifre Vidal¹

¹*Perimeter Institute for Theoretical Physics, Waterloo, Ontario N2L 2Y5, Canada*

(Dated: November 16, 2021)

The multi-scale entanglement renormalization ansatz (MERA) is a tensor network representation for ground states of critical quantum spin chains, with a network that extends in an additional dimension corresponding to scale. Over the years several authors have conjectured, both in the context of holography and cosmology, that MERA realizes a discrete version of some geometry. However, while one proposal argued that the tensor network should be interpreted as representing the hyperbolic plane, another proposal instead equated MERA to de Sitter spacetime. In this paper we show, using the framework of path integral geometry [A. Milsted, G. Vidal, arXiv:1807.02501], that MERA on the real line (and finite circle) can be given a rigorous interpretation as a two-dimensional geometry, namely a light sheet (respectively, a light cone). Accordingly, MERA describes neither the hyperbolic plane nor de Sitter spacetime. However, we also propose euclidean and lorentzian generalizations of MERA that correspond to a path integral on these two geometries.

PACS numbers: 05.30.-d, 02.70.-c, 03.67.Mn, 75.10.Jm

The multi-scale entanglement renormalization ansatz (MERA) [1–7] is a tensor network originally proposed as a variational ansatz for ground states of quantum spin chains that has over the years found a wider range of applications, including error correction [8, 9], machine learning [10–13], statistical physics [14], holography [15–18], and cosmology [19, 20]. MERA spans an additional dimension, corresponding to scale, and is particularly well-suited to describe the ground state of a critical quantum spin chain, which we can think of as a lattice version of 1+1 conformal field theory (CFT). Moreover, the network of tensors resembles a discrete version of a hyperbolic geometry. Based on these and other observations Swingle conjectured [15, 16], in a pioneering contribution that initiated a fruitful, lasting interdisciplinary discussion connecting questions in quantum gravity with tensor networks [15–42], that MERA was a lattice realization of the AdS/CFT correspondence [43–45]. Specifically, MERA on the real line would describe a time slice of the Poincaré patch of AdS₃, which corresponds to the hyperbolic plane H₂^p, with line element

$$dl(\eta, r)^2 = \left(\frac{R}{\eta}\right)^2 (d\eta^2 + dr^2) \quad (\text{hyperbolic plane}) \quad (1)$$

However, MERA is a quantum circuit that implements an entangling evolution (with time η corresponding to the renormalization group or scale direction) and, as such, is naturally equipped with a causal structure and lorentzian signature [1, 2]. This prompted Beny and several other authors, both in the context of holography [17, 18] and cosmology [19, 20], to conjecture that MERA on the real line should be interpreted instead as a Poincaré patch of de Sitter spacetime dS₂^p, with line element

$$dl(\eta, r)^2 = \left(\frac{R}{\eta}\right)^2 (-d\eta^2 + dr^2) \quad (\text{de Sitter}) \quad (2)$$

Determining which geometry, if any, MERA may describe is thus important in order to assess the potential of

this tensor network as a theoretical and numerical framework in both quantum gravity and cosmology. In this paper we establish that, when regarded as a discrete version of a CFT path integral, the geometry of MERA on the real line is that of a *light sheet* L₂^p with null scale direction η ,

$$dl(\eta, r)^2 = \frac{dr^2}{\eta^2} \quad (\text{light sheet}) \quad (3)$$

In other words, from the path integral perspective proposed in Refs. [46, 47], MERA describes neither the hyperbolic plane nor de Sitter spacetime, but an intermediate geometry with degenerate signature, see Fig. 1. This result follows from the path integral geometry of MERA *on the circle*, which we determine by studying a layer \mathcal{W} of MERA optimized for the ground state of a critical quantum spin chain. Specifically, we demonstrate that \mathcal{W} acts on the low energy states of a periodic spin chain simply as the identity map $\mathbb{1}$, which is also the map enacted by a path integral on an annulus of a *light cone* L₂. In particular, \mathcal{W} does not implement euclidean time evolution $e^{-\eta H}$ (nor real time evolution $e^{-i\eta H}$), as it would if it were a path integral on an annulus of the hyperbolic disk H₂ (respectively, of de Sitter spacetime dS₂).

We then propose two generalizations of MERA that may be useful toy models in holography and cosmology: (i) by interspersing layers \mathcal{W} with layers of *euclidean*s (tensors that implement euclidean time evolution $e^{-\eta H}$) we obtain a new tensor network representation of the CFT ground state corresponding to a path integral in the hyperbolic plane H₂; (ii) by interspersing layers \mathcal{W} with layers of *lorentzian*s (tensors that implement real time evolution $e^{-i\eta H}$) we produce a tensor network representation of the CFT ground state corresponding to a path integral in de Sitter spacetime dS₂.

Strategy.— Following Refs. [46, 47], our plan is to regard the MERA network for the ground state of a critical spin chain as a discrete, approximate CFT path integral on some geometry, and to then assign that geometry to

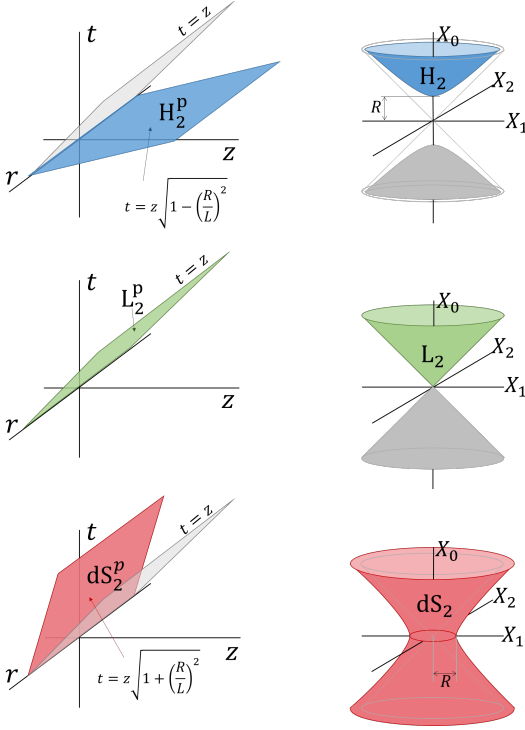


FIG. 1. (Left) Three candidate geometries for MERA on the real line, as embedded in the Poincaré patch of AdS₃ with metric $dl^2(t, z, r) = (-dt^2 + dz^2 + dr^2)/(z/L)^2$, namely the hyperbolic plane H_2^p , light sheet L_2^p , and Poincaré de Sitter dS_2^p in Eqs. (1)-(3) [58]. (Right) Three candidate geometries for MERA on the circle, as embedded in Minkowski $\mathbb{R}^{1,2}$, namely the hyperbolic disk H_2 , light cone L_2 , and de Sitter dS_2 , see Eq. (4)-(6).

MERA. Needless to say, for this strategy to make sense, the tensor network must behave as a CFT path integral in the first place. In the continuum, the path integral on a strip defines a linear map $V : \mathcal{H}_{\text{in}}^{\text{CFT}} \rightarrow \mathcal{H}_{\text{out}}^{\text{CFT}}$ between the Hilbert spaces $\mathcal{H}_{\text{in}}^{\text{CFT}}$ and $\mathcal{H}_{\text{out}}^{\text{CFT}}$ at the boundaries Σ_{in} and Σ_{out} of the strip. This linear map V enacts a conformal transformation that depends both on the geometry of the strip and on how we identified the two Hilbert spaces. On the other hand, a layer \mathcal{W} of MERA also defines a linear map, also denoted by \mathcal{W} , between the Hilbert spaces of the two spin chains at its boundaries. We can then ask whether the map \mathcal{W} matches the path integral map V for some choice of strip geometry. It is highly non-trivial that the answer is affirmative –and not only for an optimized MERA, but also for a larger class of tensor networks described in Refs. [46, 47]).

The low energy states of a critical spin chain are in one-to-one correspondence with states of a CFT [48–51]. It is thus on these states that we want to compare the action of the linear maps V and \mathcal{W} . In order to characterize the action of \mathcal{W} , we first need to explain how to relate the low energy states of the two spin chains in connects. Two difficulties lie ahead. First, in a numerical simulation of the real line (*i.e.* infinite critical spin chain), we do not

know how to reliably compute low energy states due to the absence of a mass gap in the energy spectrum. For this reason we turn to studying finite periodic spin chains instead. Second, \mathcal{W} is a coarse-graining transformation that maps states of a spin chain of size N to states of a spin chain with size $N/2$. It is therefore not obvious how to identify the two Hilbert spaces, which have very different dimension. Here we will use the techniques of Refs. [48–52] to relate each low energy state in the two spin chains through their corresponding low energy state in the CFT. With this identification, we will then be ready to numerically determine the action of \mathcal{W} and to finally compare it to candidate CFT linear maps V .

Path integral on an annulus.— We start by describing the linear map V for three candidate geometries for MERA on the circle. Consider Minkowski $\mathbb{R}^{1,2}$ with metric $dl^2 = -dX_0^2 + dX_1^2 + dX_2^2$ and the three two-dimensional manifolds given by the following constraints

$$-X_0^2 + X_1^2 + X_2^2 = -R^2 \quad (H_2) \quad (4)$$

$$-X_0^2 + X_1^2 + X_2^2 = 0 \quad (L_2) \quad (5)$$

$$-X_0^2 + X_1^2 + X_2^2 = R^2 \quad (dS_2) \quad (6)$$

see Fig. 1. We introduce polar coordinates $r = \sqrt{x^2 + y^2}$ and $\theta = \arctan(y/x)$ and use the above constraints to arrive at the metrics of the hyperbolic plane H_2 , the light cone L_2 , and the de Sitter spacetime dS_2 , namely

$$dl_{H_2}(r, \theta)^2 = \frac{1}{(r/R)^2 + 1} dr^2 + r^2 d\theta^2, \quad (7)$$

$$dl_{L_2}(r, \theta)^2 = r^2 d\theta^2, \quad (8)$$

$$dl_{dS_2}(r, \theta)^2 = \frac{-1}{(r/R)^2 - 1} dr^2 + r^2 d\theta^2. \quad (9)$$

Notice that the light cone L_2 is the limit of small radius R of both H_2 and dS_2 . For simplicity we specialize to the case $r \gg R$. A standard computation [58] shows that the CFT path integral on an annulus with boundaries given by radial coordinate r and $r/2$ produce the linear maps

$$V_{H_2} = e^{-\frac{R}{r}H} \quad (\text{euclidean}) \quad (10)$$

$$V_{L_2} = e^{0 \cdot H} = \mathbb{1} \quad (\text{null}) \quad (11)$$

$$V_{dS_2} = e^{-i\frac{R}{r}H} \quad (\text{lorentzian}) \quad (12)$$

where $H \equiv L_0 + \bar{L}_0 - c/12$ is the CFT Hamiltonian on the unit radius circle. Recall that simultaneous diagonalization of H and the momentum operator $P = L_0 - \bar{L}_0$,

$$H|\phi_\alpha^{\text{CFT}}\rangle = E_\alpha|\phi_\alpha^{\text{CFT}}\rangle, \quad P|\phi_\alpha^{\text{CFT}}\rangle = P_\alpha|\phi_\alpha^{\text{CFT}}\rangle, \quad (13)$$

yields energies E_α and momenta P_α that are given in terms of the CFT's central charge c , scaling dimensions Δ_α and conformal spins S_α according to [55–57]

$$E_\alpha = \Delta_\alpha - \frac{c}{12}, \quad P_\alpha = S_\alpha. \quad (14)$$

Map \mathcal{W} between low energy states of two spin chains.— Consider now a critical spin chain Hamiltonian $H^{(\infty)} \equiv$

$\sum_{n=-\infty}^{\infty} h_n$ on the (discrete) real line, where h_n is a local term that acts on a small neighbourhood of spin n . Following Refs. [5, 6], we obtain an approximate, scale invariant MERA representation of the ground state of $H^{(\infty)}$. The network is made of infinite layers \mathcal{W} of tensors called disentangers u and isometries w , see Fig. 2(a). Using the same optimized tensors u and w , we build a finite, periodic layer \mathcal{W} that defines a map between two periodic chains made of N and $N/2$ spins, see Fig. 2(b). The Hamiltonian $H^{(N)} \equiv \sum_{n=1}^N h_n$ on the periodic chain of size N and the one-site translation operator $T^{(N)}$ can be simultaneously diagonalized,

$$H^{(N)}|\phi_\alpha^N\rangle = E_\alpha^N|\phi_\alpha^N\rangle, \quad T^{(N)}|\phi_\alpha^N\rangle = e^{-i\frac{2\pi}{N}P_\alpha^N}|\phi_\alpha^N\rangle. \quad (15)$$

Let a_{UV} denote the lattice spacing, so that the radius of the periodic spin chain is $r = Na_{\text{UV}}/2\pi$. At low energies, after suitably normalizing h_n [59], the lattice Hamiltonian $H^{(N)}$ is a rescaled version of the CFT Hamiltonian H [48], namely $H^N \approx H/r$, and also $P^N = P$, so that

$$E_\alpha^N \approx \frac{1}{r}E_\alpha, \quad P_\alpha^N = S_\alpha \quad (16)$$

We can thus identify each eigenstate $|\phi_\alpha^N\rangle$ on the lattice with a corresponding CFT state $|\phi_\alpha^{\text{CFT}}\rangle$, that is $|\phi_\alpha^N\rangle \sim |\phi_\alpha^{\text{CFT}}\rangle$. Repeating the same procedure for the spin chain of size $N/2$, we arrive at an analogous identification $|\phi_\alpha^{N/2}\rangle \sim |\phi_\alpha^{\text{CFT}}\rangle$, which results in an identification between the low energy states of the two spin chains,

$$|\phi_\alpha^N\rangle \sim |\phi_\alpha^{N/2}\rangle. \quad (17)$$

Our goal is to then compute the matrix elements

$$\mathcal{W}_{\alpha\beta} \equiv \langle \phi_\beta^{N/2} | \mathcal{W} | \phi_\alpha^N \rangle \quad (18)$$

and, by comparison with the maps in Eqs. (19)-(12), determine whether they match any of the following options

$$(\mathcal{W})_{\alpha\beta} \stackrel{?}{\approx} (V_{\text{H}_2})_{\alpha\beta} = \delta_{\alpha\beta} e^{-\frac{R}{r}E_\alpha} \quad (\text{euclidean}) \quad (19)$$

$$(\mathcal{W})_{\alpha\beta} \stackrel{?}{\approx} (V_{\text{L}_2})_{\alpha\beta} = \delta_{\alpha\beta} \quad (\text{null}) \quad (20)$$

$$(\mathcal{W})_{\alpha\beta} \stackrel{?}{\approx} (V_{\text{ds}_2})_{\alpha\beta} = \delta_{\alpha\beta} e^{-i\frac{R}{r}E_\alpha} \quad (\text{lorentzian}) \quad (21)$$

Numerical characterization of \mathcal{W} .— As a concrete example, we have considered the critical Ising model. Given the local Hamiltonian term $h'_n = -(\sigma_n^x \sigma_{n+1}^x + \sigma_n^z)$, we produce a term h_n by suitably coarse-graining h'_n [58]. In the coarse-grained spin chain, each site is described by a vector space of dimension $\chi = 8$ and h_n acts on three consecutive sites. Upon diagonalization of $H^{(N)}$ for $N = 8$ sites, we obtain a number of low energy states $|\phi_\alpha^N\rangle$, which we organize [48–51] into the *identity*, *spin*, and *energy density* conformal towers of the Ising CFT,

$$|\mathbb{1}^N\rangle, |T^N\rangle, |\bar{T}^N\rangle, |\partial T^N\rangle, \dots \quad (\text{identity } \mathbb{1} \text{ tower}) \quad (22)$$

$$|\sigma^N\rangle, |\partial\sigma^N\rangle, |\bar{\partial}\sigma^N\rangle, \dots \quad (\text{spin } \sigma \text{ tower}) \quad (23)$$

$$|\epsilon^N\rangle, |\partial\epsilon^N\rangle, |\bar{\partial}\epsilon^N\rangle, \dots \quad (\text{energy density } \epsilon \text{ tower}) \quad (24)$$

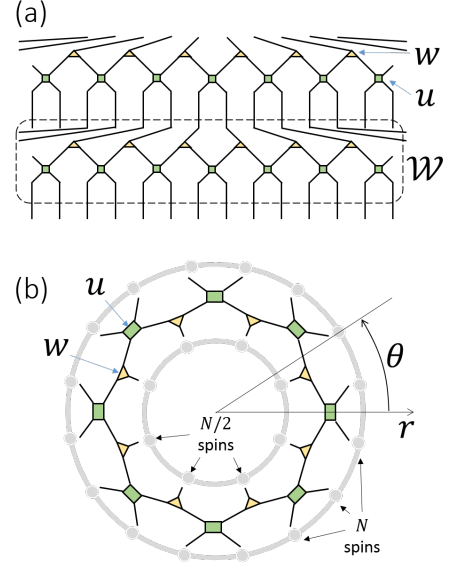


FIG. 2. (a) The MERA is made of disentangers u and isometries w organized in infinite layers \mathcal{W} . (b) A finite, periodic layer \mathcal{W} defines a linear map from the Hilbert space of a periodic spin chain with N spins to that of a smaller periodic spin chain with $N/2$ spins.

For instance, $|\mathbb{1}^N\rangle$ corresponds to the ground state of $H^{(N)}$, $|\sigma^N\rangle$ to its first excited state, and $|T^N\rangle$ is the (holomorphic) stress tensor state [55–57]. Proceeding similarly with a chain of $N/2 = 4$ sites, we obtain analogous states $|\mathbb{1}^{N/2}\rangle, |T^{N/2}\rangle, \dots$. A first numerical check confirms that \mathcal{W} is indeed diagonal in these states,

$$\mathcal{W}_{\alpha\beta} \approx \delta_{\alpha\beta} f_\alpha \quad (25)$$

in agreement with the three options (19)-(21). However, since \mathcal{W} is (by construction) an isometric map, whose eigenvalues can only either vanish or be a complex phase, we have $|f_\alpha| = 0$ or 1 , which rules out the euclidean evolution (19) corresponding to the hyperbolic disk H_2 .

To discriminate between null and lorentzian evolutions, Eqs. (20) and (21), we first need to fix the arbitrary complex phase $e^{i\varphi_\alpha^N}$ in each of state $|\phi_\alpha^N\rangle$ that appears when diagonalizing the Hamiltonian $H^{(N)}$ [60], and similarly for $H^{(N/2)}$. Fortunately, we can use recently developed techniques [50, 51] based on the Koo-Saleur formula [49], which provides a lattice version $H^{(N)} \sim L_n + \bar{L}_{-n}$ of the Virasoro generators L_n, \bar{L}_{-n} of the CFT, to establish relations between low energy states in a given conformal tower (e.g. $H_2^{(N)}|\mathbb{1}^N\rangle \approx \sqrt{c/2}|T^N\rangle$) and in this way eliminate relative complex phases (e.g. $e^{i(\varphi_1^N - \varphi_T^N)}$) within each conformal tower. Moreover, relative complex phases between different towers can be eliminated using lattice version of CFT operators [52]. After carefully eliminating all these spurious complex phases [58], the resulting matrix coefficients $\mathcal{W}_{\alpha\beta}$ are seen to coincide with the identity $\delta_{\alpha\beta}$, displaying no dependence on the energies E_α . For instance, on the 17 lowest energy eigen-

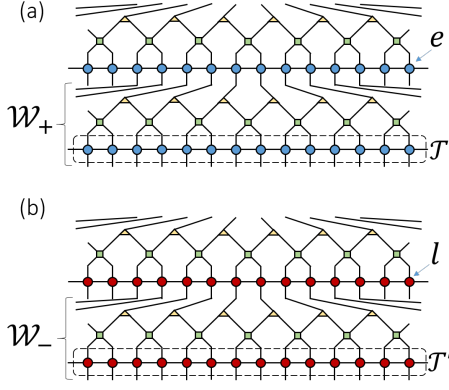


FIG. 3. (a) The euclidean MERA is a tensor network made of layers \mathcal{W} of optimized MERA interspersed with transfer matrices \mathcal{T} made of euclideanons e and implementing e^{-H} . (b) The lorentzian MERA is made of layers \mathcal{W} of optimized MERA interspersed with transfer matrices \mathcal{T}' made of lorentzions l and implementing e^{-iH} .

states of the Ising model, \mathcal{W} acts as the identity map up to corrections below 10^{-2} [58].

Geometric interpretation of the MERA.— We have thus numerically established that a periodic layer \mathcal{W} of optimized MERA implements null time evolution on the low energy states of a periodic spin chain and therefore acts as if it was a CFT path integral on an annulus of the light cone L_2 in Eq. (8). Returning to the real line, the path integral on a strip of the geometries (1)-(3) with boundaries η and 2η , where we identify the points in two boundaries points at constant value of the new space coordinate $x \equiv rR/(a_{UV}\eta)$, produces the linear maps [58]

$$V_{H_2^p} = 2^{-\frac{R}{a_{UV}}H+iD} \quad (\text{euclidean}) \quad (26)$$

$$V_{L_2^p} = 2^{iD} \quad (\text{null}) \quad (27)$$

$$V_{ds_2^p} = 2^{-i\frac{R}{a_{UV}}H+iD} \quad (\text{lorentzian}) \quad (28)$$

where now H and D are the CFT Hamiltonian and dilation operators on the real line [58]. It is well known that an infinite layer \mathcal{W} of MERA implements a rescaling transformation by a scale factor 2 [1–6]. Moreover, we have just seen on the circle that \mathcal{W} does not implement time evolution. Therefore the infinite layer \mathcal{W} of optimized MERA acts as $\mathcal{W} \approx 2^{iD}$, that is, as a CFT path integral on a strip of the light sheet L_2^p of Eq. (3). The presence of the dilation operator D in \mathcal{W} can be traced back to the identification of Hilbert spaces in the real line, which proceeds by identifying one-to-one the sites on the two infinite spin chains, in close analogy to the constant- x identification in the continuum that produces the maps (26)-(28) [58]. Notice that on the circle, a one-to-one identification between sites was not possible due to the different sizes N and $N/2$ of the spin chains, and we had to use instead the low energy spectrum identification, in close analogy to the constant- θ identification in the continuum that produces instead the maps (10)-(12).

Euclidean and lorentzian MERA.— Having numerically established the linear map implemented by a layer \mathcal{W} of optimized MERA, we can now modify the tensor network so that it implements other maps and in this way reproduce CFT path integrals on other geometries. For instance, an infinite layer $\mathcal{W}_+ \equiv \mathcal{W}\mathcal{T}$ obtained by pre-multiplying \mathcal{W} by a transfer matrix \mathcal{T} made of a row of euclideanons e , where \mathcal{T} implements an euclidean time evolution e^{-H} [46, 47], results in the linear map $V_{H_2^p}$ of Eq. (26), thus corresponding to a path integral on a strip of the hyperbolic plane H_2^p (and similarly on the circle with map V_{H_2} of Eq. (10), corresponding to a path integral on an annulus of the hyperbolic disk H_2). The resulting construction in Fig. 3(a), that we call *euclidean MERA*, closely realizes the scenario, envisaged by Swingle [15, 16], of a tensor network that represents a time slice of AdS_3 . In turn, a *lorentzian MERA* is obtained using instead layers $\mathcal{W}_- \equiv \mathcal{W}\mathcal{T}'$, see Fig. 3(b), where \mathcal{T}' is made of a row of lorentzions l and implements a lorentzian time evolution e^{-iH} [58]. \mathcal{W}_- is then seen to implement the linear map $V_{ds_2^p}$ of Eq. (28), thus corresponding to a path integral on a strip of the Poincare de Sitter spacetime ds_2^p (and similarly on the circle), thus closely realizing the scenario, envisaged by Cedric and other authors [17–20], of a tensor network that represents de Sitter spacetime.

Discussion.— In this work we have assigned a path integral geometry to the (null, euclidean, and lorentzian) MERA starting from three candidate geometries and enforcing only rule 1 of Ref. [47], which demands “consistency between the path integral map V and the tensor network map \mathcal{W} ”. However, a local rescaling $g_{\mu\nu}(\eta, r) \rightarrow g'_{\mu\nu}(\eta, r) = \Omega(\eta, r)^2 g_{\mu\nu}(\eta, r)$ in a CFT leaves the map V essentially unchanged, so that a geometric assignment based on rule 1 of Ref. [47] alone only determines the conformal class of the metric $g_{\mu\nu}$. However, we can now fix the scale factor $\Omega(\eta, r)$ and recover the geometries in Eqs. 1-3 and 7-9 (that is, without preassuming them as candidates) by enforcing rule 2 of Ref. [47], which states that “the lattice spacing is the same constant a_{UV} throughout the tensor network” [58].

In summary, we have numerically established that a MERA optimized to represent the ground state of a critical quantum spin chain on the circle / real line behaves as a CFT path integral on a light cone / light sheet geometry. Moreover, we have proposed two new tensor networks that correspond to hyperbolic space and de Sitter spacetime, thus realizing previously conjectured constructions. Particularly intriguing is the optimized MERA refusal to perform real time evolution (something that is in principle possible within the MERA variational class), suggesting that the optimal preparation of a CFT ground state through a path integral [37–42, 61–64] does not actually require time evolution [66]. Perhaps even more tantalizing is the fact that the tensor networks discussed above open a new venue to numerically simulate quantum field theories in curved spacetime [67].

Acknowledgments. The authors thank Bartłomiej

Czech, Pawel Caputa, Olalla Castro-Alvaredo, William Donnelly, Benjamin Doyon, Davide Gaiotto, Qi Hu, Lampros Lamprou, Juan Maldacena, David Mateos, Samuel McCandlish, James Sully, Vasudev Shyam, Tadashi Takayanagi, and Xiao-liang Qi for fruitful discussions and feedback. Very special thanks go to Ling-Yan (Janet) Hung and Rob Myers for their patient, tenacious attempt to teach us CFT and curved spacetime background ma-

terial. The authors acknowledge support by the Simons Foundation (Many Electron Collaboration), by NSERC (discovery grant), and by Compute Canada. Research at Research at Perimeter Institute is supported by the Government of Canada through the Department of Innovation, Science and Economic Development Canada and by the Province of Ontario through the Ministry of Research, Innovation and Science.

-
- [1] G. Vidal, *Entanglement renormalization*, Phys. Rev. Lett. 99, 220405 (2007), arXiv:cond-mat/0512165.
 - [2] G. Vidal, *A class of quantum many-body states that can be efficiently simulated*, Phys. Rev. Lett. 101, 110501 (2008), arXiv:quant-ph/0610099.
 - [3] G. Evenbly, G. Vidal, *Algorithms for entanglement renormalization* Phys. Rev. B 79 (14), 144108 (2009), arXiv:0707.1454.
 - [4] V. Giovannetti, S. Montangero, R. Fazio *Quantum Multiscale Entanglement Renormalization Ansatz Channels* Phys. Rev. Lett. 101, 180503 (2009), arXiv:0804.0520.
 - [5] R. N. C. Pfeifer, G. Evenbly, G. Vidal *Entanglement renormalization, scale invariance, and quantum criticality*, Phys. Rev. A 79(4), 040301(R) (2009), arXiv:0810.0580.
 - [6] G. Evenbly, G. Vidal, *Quantum Criticality with the Multi-scale Entanglement Renormalization Ansatz*, chapter 4 of "Strongly Correlated Systems. Numerical Methods" (Springer Series in Solid-State Sciences, Vol. 176 2013), arXiv:1109.5334
 - [7] M. Aguado, G. Vidal *Entanglement renormalization and topological order*, Phys. Rev. Lett. 100, 070404 (2008), arXiv:0712.0348
 - [8] A. J. Ferris, D. Poulin *Tensor Networks and Quantum Error Correction*, Phys. Rev. Lett. 113, 030501(2014), arXiv:1312.4578.
 - [9] A.J. Ferris, D. Poulin, *Branching MERA codes: A natural extension of classical and quantum polar codes*, Information Theory (ISIT), 2014 IEEE International Symposium on, 1081-1085.
 - [10] C. Beny, *Deep learning and the renormalization group*, arXiv:1301.3124
 - [11] E.M. Stoudenmire, D.J. Schwab *Supervised Learning with Quantum-Inspired Tensor Networks*, Advances in Neural Information Processing Systems 29, 4799 (2016), arXiv:1605.05775.
 - [12] Y. Levine, O. Sharir, N. Cohen, A. Shashua, *Bridging Many-Body Quantum Physics and Deep Learning via Tensor Networks*, arXiv:1803.09780.
 - [13] I. Cong, S. Choi, M. D. Lukin, *Quantum Convolutional Neural Networks*, arXiv:1810.03787
 - [14] G. Evenbly, G. Vidal *Tensor network renormalization yields the multi-scale entanglement renormalization ansatz*, Phys. Rev. Lett. 115, 200401 (2015), arXiv:1502.05385
 - [15] B. Swingle, *Entanglement Renormalization and Holography*, Phys. Rev. D 86, 065007 (2012), arXiv:0905.1317.
 - [16] B. Swingle, *Constructing holographic spacetimes using entanglement renormalization*, arXiv:1209.3304.
 - [17] C. Beny, *Causal structure of the entanglement renormalization ansatz*, New J. Phys. 15 (2013) 023020, arXiv:1110.4872.
 - [18] B. Czech, L. Lamprou, S.I McCandlish, and J. Sully, *Tensor Networks from Kinematic Space*, JHEP07 (2016) 100, arXiv:1512.01548.
 - [19] R.S. Kunkolienkar, K. Banerjee, *Towards a dS/MERA correspondence*, Int. J. Mod. Phys. D 26, 1750143 (2017), arXiv:1611.08581.
 - [20] N. Bao, C. Cao, S. M. Carroll, A. Chatwin-Davies, *De Sitter space as a tensor network: Cosmic no-hair, complementarity, and complexity*, Phys. Rev. D 96, 123536 (2017), arXiv:1709.03513.
 - [21] X.-L. Qi, *Exact holographic mapping and emergent space-time geometry*, arXiv:1309.6282.
 - [22] C. H. Lee, X.-L. Qi *Exact holographic mapping in free fermion systems*, Phys. Rev. B 93,035112 (2016), arXiv:1503.08592.
 - [23] F. Pastawski, B. Yoshida, D. Harlow, J. Preskill, *Holographic quantum error-correcting codes: Toy models for the bulk/boundary correspondence*, JHEP 06 (2015) 149, arXiv:1503.06237.
 - [24] P. Hayden, S. Nezami, X.-L. Qi, N. Thomas, M. Walter, Z. Yang, *Holographic duality from random tensor networks*, JHEP 11 (2016) 009, arXiv:1601.01694.
 - [25] X.-L. Qi, Z. Yang, *Space-time random tensor networks and holographic duality*, arXiv:1801.05289.
 - [26] J. Haegeman, T. J. Osborne, H. Verschelde and F. Verstraete, *Entanglement Renormalization for Quantum Fields in Real Space*, Phys. Rev. Lett., 110, 100402 (2013), arXiv:1102.5524
 - [27] A. Mollabashi, M. Naozaki, S. Ryu and T. Takayanagi, *Holographic geometry of cMERA for quantum quenches and finite temperature*, JHEP (2014) 2014: 98, arXiv:1311.6095.
 - [28] M. Nozaki, S. Ryu and T. Takayanagi, *Holographic geometry of entanglement renormalization in quantum field theories*, JHEP (2012) 2012: 10, arXiv:1208.3469.
 - [29] J. Molina-Vilaplana, *Information geometry of entanglement renormalization for free quantum fields*, JHEP (2015) 2015:2 (mar, 2015), arXiv:1503.07699.
 - [30] J. Molina-Vilaplana, *Entanglement renormalization and two dimensional string theory*, Phys. Lett. B 755 (2016) 421-425, arXiv:1510.09020.
 - [31] M. Miyaji, S. Ryu, T. Takayanagi and X. Wen, *Boundary states as holographic duals of trivial spacetimes*, JHEP (2015) 2015: 152, arXiv:1412.6226.
 - [32] M. Miyaji, T. Numasawa, N. Shiba, T. Takayanagi, K. Watanabe, *cMERA as Surface/State Correspondence in AdS/CFT*, Phys. Rev. Lett. 115, 171602 (2015), arXiv:1506.01353.
 - [33] M. Miyaji and T. Takayanagi, *Surface/state correspondence as a generalized holography*, Progress of Theo-

- retical and Experimental Physics 2015 (mar, 2015) , arXiv:1503.03542.
- [34] X. Wen, G. Y. Cho, P. L. S. Lopes, Y. Gu, X. L. Qi and S. Ryu, *Holographic entanglement renormalization of topological insulators*, Phys. Rev. B 94, 075124 (2016), arXiv:1605.07199.
- [35] J. R. Fliss, R. G. Leigh and O. Parrikar, *Unitary Networks from the Exact Renormalization of Wave Functionals*, Phys. Rev. D 95, 126001 (2017), arXiv:1609.03493.
- [36] G. Evenbly, G. Vidal, *Tensor network renormalization*, Phys. Rev. Lett. 115 (18), 180405 (2015), arXiv:1412.0732.
- [37] M. Miyaji, T. Takayanagi, K. Watanabe, *From Path Integrals to Tensor Networks for AdS/CFT*, Phys. Rev. D 95, 066004 (2017), arXiv:1609.04645.
- [38] P. Caputa, N. Kundu, M. Miyaji, T. Takayanagi, K. Watanabe, *Anti-de Sitter Space from Optimization of Path Integrals in Conformal Field Theories*, Phys. Rev. Lett. 119, 071602 (2017), arXiv:1703.00456.
- [39] P. Caputa, N. Kundu, M. Miyaji, T. Takayanagi, K. Watanabe, *Liouville Action as Path-Integral Complexity: From Continuous Tensor Networks to AdS/CFT*, JHEP 11(2017)097, arXiv:1706.07056.
- [40] B. Czech, *Einstein's equations from Varying Complexity*, Phys. Rev. Lett. 120, 031601 (2018), arXiv:1706.00965.
- [41] P. Caputa, J. M. Magan, *Quantum Computation as Gravity*, arXiv:1807.04422.
- [42] T. Takayanagi, *Holographic Spacetimes as Quantum Circuits of Path-Integrations*, arXiv:1808.09072
- [43] J.M. Maldacena, *The Large N Limit of Superconformal Field Theories and Supergravity*, Adv. Theor. Math. Phys. 2:231-252 (1998), arXiv:hep-th/9711200.
- [44] S. S. Gubser, I. R. Klebanov, and A. M. Polyakov, *Gauge Theory Correlators from Non-Critical String Theory*, Phys. Lett. B 428, 105 (1998), arXiv:hep-th/9802109.
- [45] E. Witten, *Anti De Sitter Space And Holography*, Adv. Theor. Math. Phys. 2, 253 (1998), arXiv:hep-th/9802150.
- [46] A. Milsted, G. Vidal, *Tensor networks as conformal transformations*, arXiv:1805.12524
- [47] A. Milsted, G. Vidal, *Tensor networks as path integral geometry*, arXiv:1807.02501
- [48] J. L. Cardy, *Conformal invariance and universality in finite-size scaling*, J. Phys. A: Math. Gen. 17, L385 (1984).
- [49] W. M. Koo and H. Saleur, *Representations of the Virasoro algebra from lattice models*, Nucl. Phys. B 426, 459 (1994), arXiv:hep-th/9312156.
- [50] A. Milsted, G. Vidal, *Extraction of conformal data in critical quantum spin chains using the Koo-Saleur formula*, Phys. Rev. B 96, 245105 (2017), arXiv:1706.01436
- [51] Y. Zou, A. Milsted, G. Vidal, *Conformal data and renormalization group flow in critical quantum spin chains using periodic uniform matrix product states*, arXiv:1710.05397
- [52] Y. Zou, A. Milsted, G. Vidal, *Conformal fields and operator product expansion in critical quantum spin chains*, In preparation.
- [53] G. Evenbly, *Algorithms for tensor network renormalization* Phys. Rev. B 95, 045117 (2017), arXiv:1509.07484.
- [54] G. Evenbly, G. Vidal *Local scale transformations on the lattice with tensor network renormalization*, Phys. Rev. Lett. 116, 040401 (2016), arXiv:1510.00689.
- [55] P. Ginsparg, *Applied Conformal Field Theory*, arXiv:hep-th/9108028 (1988).
- [56] P. Di Francesco, P. Mathieu, and D. Senechal, *Conformal Field Theory* (Springer, New York, 2012).
- [57] M. Henkel, *Conformal Invariance and Critical Phenomena*, (Springer, New York, 1999).
- [58] See appendices below for further details.
- [59] The local Hamiltonian term h_n is normalized (by a constant shift and a rescaling, $h_n \rightarrow a + b h_n$, where the constants a and b are independent of the size N of the spin chain) such that the low energy spectrum matches that of a CFT on a circle of length Na_{UV} , or radius $r = Na_{UV}/2\pi$, where a_{UV} is the lattice spacing.
- [60] If $|\psi_\alpha^N\rangle$ is a normalized eigenstate of $H^{(N)}$, with $H^{(N)}|\psi_\alpha^N\rangle = E_\alpha^N|\psi_\alpha^N\rangle$, then so is $e^{i\varphi_\alpha^N}|\psi_\alpha^N\rangle$ for any angle $\varphi_\alpha^N \in [0, 2\pi)$. Therefore by diagonalizing $H^{(N)}$ we obtain (normalized) energy eigenvectors $|\psi_\alpha^N\rangle$ that are only defined up to an arbitrary complex phase $e^{i\varphi_\alpha^N}$.
- [61] D. Stanford, L. Susskind, *Complexity and shock wave geometries*, Phys. Rev. D 90, 126007 (2014), arXiv:1406.2678.
- [62] A. R. Brown, D. A. Roberts, L. Susskind, B. Swingle, Y. Zhao, *Complexity, action, and black holes*, Phys. Rev. D 93, 086006 (2016), arXiv:1512.04993.
- [63] A. R. Brown, D. A. Roberts, L. Susskind, B. Swingle, Y. Zhao, *Holographic complexity equals bulk action?*, Phys. Rev. Lett. 116, 191301 (2016), arXiv:1509.07876.
- [64] R. Jefferson, R. C. Myers, *Circuit complexity in quantum field theory*, JHEP10(2017)107, arXiv:1707.08570
- [65] S. Chapman, J. Eisert, L. Hackl, M. P. Heller, R. Jefferson, H. Marrochio, R. C. Myers, *Complexity and entanglement for thermofield double states*, arXiv:1810.05151
- [66] J. Sully, R. Myers, G. Vidal, *The true truth about CFT complexity*, in eternal preparation.
- [67] A. Lewis, Q. Hu, G. Vidal, *Tensor networks for quantum field theories in curved spacetime*, in preparation.

I. APPENDIX: MERA ON THE CIRCLE

In this Appendix we review how to assign a path integral geometry to the *periodic* MERA, which is a tensor network used to represent the ground state of a critical quantum spin chain *on the circle*. We consider both the usual MERA (in what follows named *null* MERA) as well as the two extensions proposed in the main text, namely the *euclidean* MERA and the *lorentzian* MERA, see Fig. 4. We have argued that, from a path integral perspective, the periodic version of these tensor networks represent the following geometries:

null MERA \mathcal{M}	\leftrightarrow	light cone L_2	(29)
euclidean MERA \mathcal{M}_+	\leftrightarrow	hyperbolic space H_2	
lorentzian MERA \mathcal{M}_-	\leftrightarrow	de Sitter spacetime dS_2	

In euclidean and lorentzian MERA, this geometry assignment holds in the limit when the radial coordinate r of H_2 or dS_2 is much larger than some radius R (see below).

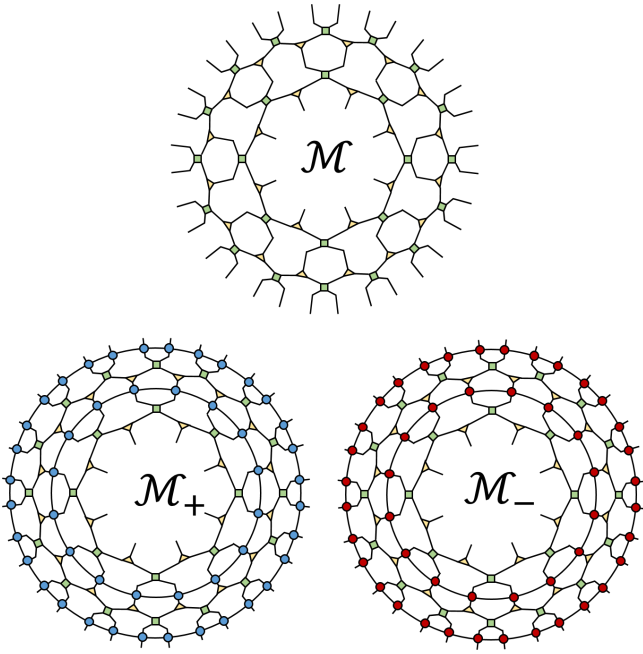


FIG. 4. Graphical representation of several MERA tensor networks on the circle (only two concentric layers of each different MERA are displayed). Top: null MERA \mathcal{M} , with layers \mathcal{W} made of disentangers and isometries. Bottom left: euclidean MERA \mathcal{M}_+ , with layers $\mathcal{W}_+ = \mathcal{W}\mathcal{T}^q$ (for $q = 1$), where \mathcal{T} is an euclidean transfer matrix that implements euclidean time evolution. Bottom right: lorentzian MERA \mathcal{M}_- , with layers $\mathcal{W}_- = \mathcal{W}\mathcal{T}_-^q$ (for $q = 1$), where \mathcal{T}_- is a lorentzian transfer matrix that implements real time evolution.

We start by reviewing how the three geometries H_2 , dS_2 , and L_2 can be embedded in a common three-dimensional ambient space, namely Minkowski $\mathbb{R}^{1,2}$ (see Appendix III for a review of similar embeddings when the ambient space is AdS_3). Then we characterize the different linear maps obtained through a CFT path integral on an annulus of the H_2 , dS_2 , and L_2 geometries. These linear maps correspond to time evolution of three types: euclidean, lorentzian, and no time evolution, respectively. Finally, using the two rules of Ref. [47] to assign a *path integral* geometry to a tensor network, we establish that a periodic layer of euclidean, lorentzian, and null MERA corresponds to an annulus of the H_2 , dS_2 , and L_2 geometries, respectively.

The geometry and path integral derivations reviewed in this Appendix are all well-known but scattered through the literature. The characterization of the linear maps, and the corresponding identification with specific tensor networks, are a particular case (translation invariant maps and networks) of the formalism recently presented in Ref. [47] (which also applies more broadly to inhomogeneous maps and networks).

Remark on notation: In this paper we use L_2^p , H_2^p , and dS_2^p (that is, with the superscript p) to denote the *Poincare patch* or *local coordinate* version of the L_2 , H_2 , and dS_2 geometries, namely a light sheet, the hyper-

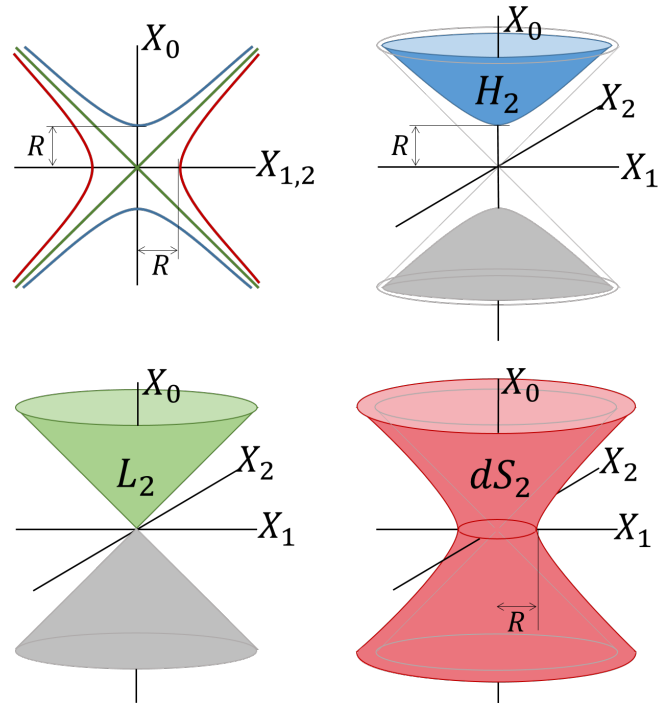


FIG. 5. The three geometries H_2 , dS_2 , and L_2 of interest are shown embedded in three-dimensional Minkowski spacetime $\mathbb{R}^{1,2}$ with time coordinate X_0 and space coordinates X_1 and X_2 , according to the restrictions (31)-(33). Notice that both H_2 and dS_2 depend on a radius R , and that L_2 can be understood as the limit $R \rightarrow 0$ of either of these two geometries, see Fig. 6.

bolic plane, and the Poincare patch of de Sitter spacetime. These are the geometries corresponding to null, euclidean, and lorentzian MERA when the tensor network describes the ground state of a critical spin chain *on the line*, and will be addressed in Appendix (II).

A. Embeddings in Minkowski $\mathbb{R}^{1,2}$

A useful characterization of the geometries H_2 , dS_2 , and L_2 is as two-dimensional embeddings in three-dimensional Minkowski spacetime $\mathbb{R}^{1,2}$. Let X_0 denote the time coordinate and X_1 and X_2 the two space coordinates, and recall that the metric of $\mathbb{R}^{1,2}$ reads, when expressed as a squared line element dl^2 ,

$$dl^2 = -dX_0^2 + dX_1^2 + dX_2^2. \quad (30)$$

Then H_2 , dS_2 , and L_2 are given by the constraints

$$-X_0^2 + X_1^2 + X_2^2 = -R^2 \quad (H_2), \quad (31)$$

$$-X_0^2 + X_1^2 + X_2^2 = R^2 \quad (dS_2), \quad (32)$$

$$-X_0^2 + X_1^2 + X_2^2 = 0 \quad (L_2), \quad (33)$$

where R is the radius of curvature, see Fig. 5.

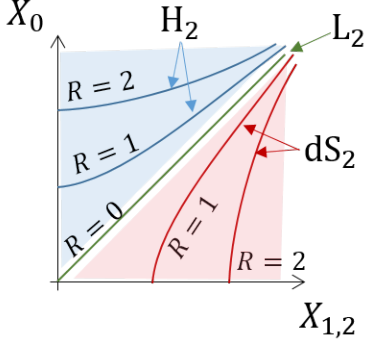


FIG. 6. The light cone geometry L_2 can be understood as the zero radius limit $a \rightarrow 0$ of both the Poicare disk H_2 and global de Sitter space dS_2 , as can be seen when considering these two-dimensional geometries as embedded in Minkowski $\mathbb{R}^{1,2}$, where X_0 is the time coordinate and X_1 and X_2 are space coordinates.

We can use polar coordinates

$$r = \sqrt{X_1^2 + X_2^2}, \quad \theta = \arctan(X_2/X_1), \quad (34)$$

where $r \geq 0$ and $\theta \in [0, 2\pi)$, or

$$X_1 = r \cos(\theta), \quad X_2 = r \sin(\theta), \quad (35)$$

to rewrite the metric on $\mathbb{R}^{1,2}$ and the constraints as

$$dl^2 = -dX_0^2 + dr^2 + r^2 d\theta^2, \quad (36)$$

and

$$-X_0^2 + r^2 = -R^2 \quad (H_2), \quad (37)$$

$$-X_0^2 + r^2 = R^2 \quad (dS_2), \quad (38)$$

$$-X_0^2 + r^2 = 0 \quad (L_2), \quad (39)$$

and then use these constraints to arrive to the following induced metrics

$$dl_{H_2}^2 = \frac{dr^2}{(r/R)^2 + 1} + r^2 d\theta^2, \quad (40)$$

$$dl_{dS_2}^2 = \frac{-dr^2}{(r/R)^2 - 1} + r^2 d\theta^2, \quad (41)$$

$$dl_{L_2}^2 = r^2 d\theta^2, \quad (42)$$

where $r^2 \geq 0$, $r^2 \geq R^2$, and $r^2 \geq 0$, respectively. Notice that the light cone L_2 is the limit of small radius R , $\lim R \rightarrow 0$, of both the hyperbolic plane H_2 and de sitter spacetime dS_2 , see Fig. 6.

The coordinate system (r, θ) makes manifest the invariance of these three manifolds under θ rotations of the $X_1 X_2$ plane. However, as the above embeddings suggest, these three two-dimensional manifolds are also invariant under the larger $SO(1, 2)$ group of isometries of Minkowski $\mathbb{R}^{1,2}$, which includes two more generators (Lorentz boosts in the $X_0 X_1$ and $X_0 X_2$ planes).

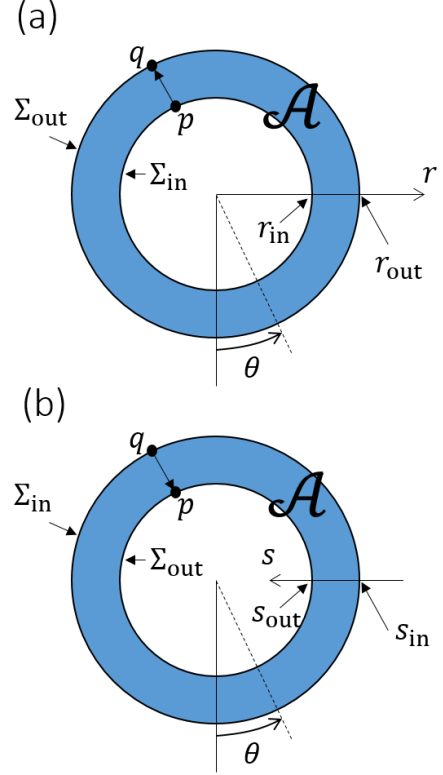


FIG. 7. (a) Annulus \mathcal{A} with boundaries Σ_{in} and Σ_{out} corresponding to circles of radius $r = r_{\text{in}}$ and $r = r_{\text{out}}$ where $r_{\text{in}} < r_{\text{out}}$. The constant- θ identification identifies point $p \in \Sigma_{\text{in}}$ with point $q \in \Sigma_{\text{out}}$. (b) Same annulus \mathcal{A} as before but with different radial coordinate s , which grows when the radius of the circle decreases. Notice that the names of the boundaries of the annulus have swapped. Σ_{in} and Σ_{out} now correspond to values $s = s_{\text{in}}$ and $s = s_{\text{out}}$ with $s_{\text{in}} < s_{\text{out}}$.

B. Linear map by path integral on an annulus

The above geometries H_2 , dS_2 , and L_2 can all be sliced into slices Σ_r defined by a constant value of the radial coordinate r . Each slice Σ_r corresponds to a circle of length $2\pi r$. Two concentric circles with radii r_{in} and r_{out} , with $r_{\text{in}} > r_{\text{out}}$, define an annulus \mathcal{A} characterized by $r \in [r_{\text{out}}, r_{\text{in}}]$, $\theta \in [0, 2\pi)$, see Fig. 7(a).

Consider now a two-dimensional CFT with field ϕ and action functional $S[\phi]$. In any of the three geometries, given the circle Σ_{in} for $r = r_{\text{in}}$, we can define the Hilbert space $\mathcal{H}(\Sigma_{\text{in}})$ of the CFT on that circle in terms of basis states $|\varphi(\theta)\rangle$. Here $\varphi(\theta)$, for $\theta \in [0, 2\pi)$, is a field configuration that results from restricting the field $\phi(r, \theta)$ to the circle Σ_{in} . We can similarly define the Hilbert space $\mathcal{H}(\Sigma_{\text{out}})$ of the CFT on a second circle Σ_{out} given by $r = r_{\text{out}}$, again with basis $|\varphi(\theta)\rangle$. We can then identify the two Hilbert spaces \mathcal{H}_{in} and \mathcal{H}_{out} (from now on simply \mathcal{H}) by identifying basis vectors according to

$$|\varphi(\theta)\rangle_{\Sigma_{\text{in}}} \sim |\varphi'(\theta)\rangle_{\Sigma_{\text{out}}}, \text{ iff } \varphi(\theta) = \varphi'(\theta) \text{ for all } \theta. \quad (43)$$

For concreteness, from now on we continue the discussion for the hyperbolic geometry H_2 , and we postpone the analysis of dS_2 and L_2 to parts (IM) and (IN) of this Appendix. We introduce the linear map $V : \mathcal{H} \rightarrow \mathcal{H}$ given by the path integral on an annulus \mathcal{A} of H_2 , that is with matrix elements

$$\langle \varphi'(\theta) | V | \varphi(\theta) \rangle = \int [D\phi] e^{-S[\phi(r,\theta)]}. \quad (44)$$

In this expression the integral is over field configurations $\phi(r, \theta)$ restricted to the annulus \mathcal{A} and with boundary conditions $\varphi(\theta)$ and $\varphi'(\theta)$,

$$\phi(r_{\text{in}}, \theta) = \varphi(\theta), \quad \phi(r_{\text{out}}, \theta) = \varphi'(\theta), \quad (45)$$

whereas $[D\phi]$ and $S[\phi(r, \theta)]$ are the integration measure and the *euclidean* action of the CFT.

C. Thin annulus

In the limit of a thin annulus, when $r_{\text{in}} - r_{\text{out}} = \epsilon$ for small $\epsilon > 0$, we can expand the linear map $V \approx \mathbb{1} - \epsilon Q$ in terms of a generator Q . An expression for Q is found by specializing to the current case the general solution derived in Ref. [47] and reviewed in Appendix (IV). For a diagonal metric of the form

$$dl^2 = \Omega^2(r) (a(r)^2 dr^2 + d\theta^2) \quad (46)$$

this generator is

$$Q = a(r) \int_0^{2\pi} d\theta h(\theta) = a(r) H_0, \quad (47)$$

$$H_0 \equiv \int_0^{2\pi} d\theta h(\theta) = L_0 + \bar{L}_0 - \frac{c}{12}, \quad (48)$$

where H_0 is the CFT Hamiltonian H_0 on a circle of unit radius. Its spectrum of energies E_α is given in terms of the scaling dimensions Δ_α of local scaling fields by $E_\alpha = \Delta_\alpha - c/12$. That is, the path integral linear map V is an euclidean time evolution as generated by the CFT Hamiltonian H_0 .

Specifically, for the hyperbolic space H_2 in coordinates (r, θ) we have

$$a(r) = \frac{R}{r\sqrt{r^2 + R^2}}. \quad (49)$$

For later reference, we quote the resulting metric and generator Q :

$$dl_{H_2}^2 = \frac{R^2 dr^2}{r^2 + R^2} + r^2 d\theta^2 \quad (50)$$

$$= r^2 \left(\frac{R^2 (dr/r)^2}{(r^2 + R^2)} + d\theta^2 \right), \quad (51)$$

$$Q_{H_2} = \frac{R}{r\sqrt{r^2 + R^2}} H_0. \quad (52)$$

D. The $r \gg R$ regime

Of particular importance for our discussion is the H_2 geometry in the regime of large radial coordinate r , that is when $r \gg R$, since it is in this regime that the connection to euclidean MERA is most transparent. In addition, in this regime computations become simpler. To leading order in r/R , the metric and generator simplify to

$$dl_{H_2}^2 \approx \frac{R^2 dr^2}{r^2} + r^2 d\theta^2 \quad (53)$$

$$= r^2 \left(\frac{R^2 dr^2}{r^4} + d\theta^2 \right), \quad (54)$$

$$Q_{H_2} \approx \frac{R}{r^2} H_0. \quad (55)$$

E. Thick annulus

The path integral on a thick annulus $r \in [r_{\text{in}}, r_{\text{out}}]$ for $r_{\text{in}} \gg R$ corresponds to the finite linear map

$$V_{H_2} = \mathcal{P} \exp \left(- \int_{r_{\text{in}}}^{r_{\text{out}}} dr Q_{H_2} \right) \quad (56)$$

$$\approx \exp \left(- H_0 \int_{r_{\text{in}}}^{r_{\text{out}}} \frac{R dr}{r^2} \right) \quad (57)$$

$$= \exp \left(- \frac{R(r_{\text{out}} - r_{\text{in}})}{r_{\text{in}} r_{\text{out}}} H_0 \right), \quad (58)$$

where we used

$$\int_{r_{\text{in}}}^{r_{\text{out}}} \frac{R dr}{r^2} = \frac{-R}{r} \Big|_{r_{\text{in}}}^{r_{\text{out}}} = -R \left(\frac{1}{r_{\text{out}}} - \frac{1}{r_{\text{in}}} \right). \quad (59)$$

F. Another useful radial coordinate

Let us consider a second radial coordinate s , given in terms of r by

$$r = r_0 e^{-s}, \quad \text{or} \quad s = \log(r_0/r), \quad (60)$$

where r_0 is a reference radius and s is dimensionless. The metric of H_2 , the generator Q_{H_2} , and the finite gate V_{H_2} read, in the simplifying regime $r \gg R$,

$$dl_{H_2}^2 \approx R^2 ds^2 + r_0^2 e^{-2s} d\theta^2 \quad (61)$$

$$= r_0^2 e^{-2s} \left(\left(\frac{R}{r_0} \right)^2 e^{2s} dz^2 + d\theta^2 \right), \quad (62)$$

$$Q_{H_2} \approx \frac{R}{r_0} e^s H_0, \quad (63)$$

$$V_{H_2} = \mathcal{P} \exp \left(- \int_{s_{\text{in}}}^{s_{\text{out}}} ds Q_{H_2} \right) \quad (64)$$

$$\approx \exp \left(- \int_{s_{\text{in}}}^{s_{\text{out}}} ds \frac{R}{r_0} e^s H_0 \right) \quad (65)$$

$$= \exp \left(- (e^{s_{\text{out}}} - e^{s_{\text{in}}}) \frac{R}{r_0} H_0 \right). \quad (66)$$

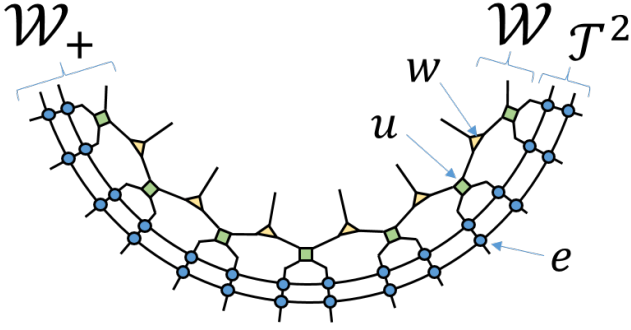


FIG. 8. Layer \mathcal{W}_+ of euclidean MERA on the circle. Only part of this periodic layer is shown. \mathcal{W}_+ is made of the product of q periodic euclidean transfer matrices \mathcal{T} ($q = 2$ in the figure) and a layer \mathcal{W} of null or regular MERA, see Eq. (67). Each euclidean transfer matrix \mathcal{T} consist of the product of a periodic chain of tensors e called euclideanons. Each layer \mathcal{W} of null MERA is made of tensors u and w called disentanglers and isometries.

Notice that while the radial coordinate r measures the proper length of the circle Σ_r , in that the proper length of Σ_r is $2\pi r$, see Eq. (50), in the regime $r \gg R$ the merit of the radial coordinate s is that it is proportional to proper euclidean time. Indeed, Eq. (61) reveals that the proper euclidean time is measured by $s' \equiv Rs$. In particular, s will be seen to be a natural radial coordinate to count layers of the euclidean MERA.

G. Linear map of \mathcal{W}_+ on the circle

Next we identify what linear map is implemented by a periodic layer \mathcal{W}_+ of euclidean MERA made of q copies of the periodic euclidean transfer matrix \mathcal{T} and a periodic layer \mathcal{W} of MERA,

$$\mathcal{W}_+ \equiv \mathcal{W}\mathcal{T}^q, \quad (67)$$

see Fig. 8. We think of the layer \mathcal{W}_+ as a linear map from the lower spin chain made of N sites to the upper spin chain made of $N/2$ sites.

The euclidean transfer matrix \mathcal{T} is a tensor network, consisting of a periodic row of euclideanons, that acts on the Hilbert space of a periodic quantum spin chain made of N spins. By construction, it implements an euclidean time evolution of the form

$$\mathcal{T} \approx \exp(-H(N)) = \exp\left(-\frac{2\pi}{N}H_0\right), \quad (68)$$

where the spin chain Hamiltonian

$$H(N) \equiv \sum_{l=1}^N h_l, \quad (69)$$

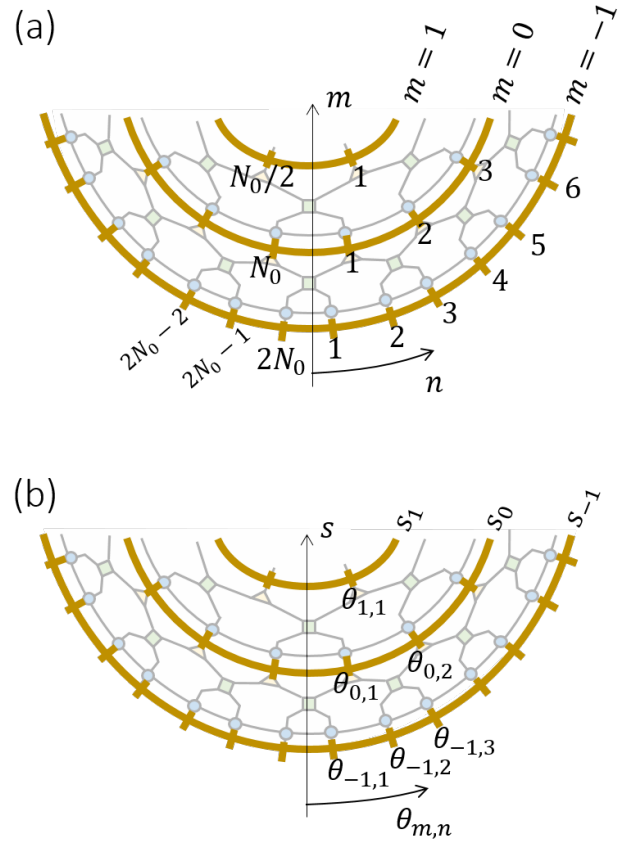


FIG. 9. (a) We label each spin chain between two layers of euclidean MERA by an integer m , and each site within that spin chain by the pair (m, n) . (b) We then assign to site (m, n) discrete coordinates $(s_m, \theta_{m,n})$ as given by (73).

acts approximately as $H(N) \approx (2\pi/N)(L_0 + \bar{L}_0 - c/12)$ on low energy states, up to corrections that are subleading in $1/N$. On the other hand, as shown in this paper and further detailed in Appendix (V), a periodic layer \mathcal{W} of null MERA defines a linear map from (the Hilbert space of a periodic spin chain made of) N spins into (the Hilbert space of a periodic spin chain made of) $N/2$ spins that acts on low energy states as the identity operator,

$$\mathcal{W} \approx \mathbb{1}. \quad (70)$$

We conclude that a layer \mathcal{W}_+ of euclidean MERA maps states of N spins into states of $N/2$ spins while implementing the linear map

$$\mathcal{W}_+ = \mathcal{W}\mathcal{T}^q = \mathbb{1} \times \exp(-qH(N)) \quad (71)$$

$$\approx \exp\left(-q\frac{2\pi}{N}H_0\right) \quad (72)$$

on low energy states.

H. Discrete coordinates on the euclidean MERA

Consider the euclidean MERA on the circle. We label the spin chains between layers of euclidean MERA by an integer m . If the spin chain $m = 0$ has N_0 sites (which we assume to be divisible by a large power of 2), then the spin chain $m = 1$ has $N_1 = N_0/2$ sites. More generally, the spin chain m has $N_m = N_0 2^{-m}$ sites. We label the sites in the spin chain m by a second integer $n \in \{1, \dots, N_m\}$. Therefore each site of any spin chain is assigned a unique pair (m, n) of integers, see Fig. 9(a). We then further assign discrete radial and angular coordinate $(s_m, \theta_{m,n})$ to site (m, n) according to

$$s_m \equiv m \log 2, \quad \theta_{m,n} \equiv \frac{2\pi}{N_m} \left(n - \frac{1}{2} \right), \quad (73)$$

see Fig. 9(b).

Let us consider a candidate geometry for the euclidean MERA in the regime $N_m \gg 2\pi q$ (which will turn out to correspond to the regime $r \gg R$ or $s \ll \log(r_0/R)$ in H_2). It is initially given by a generic metric in radial and angular coordinates (s, θ) , which can always be written as (see Appendix (IV))

$$dl^2 = \Omega(s, \theta)^2 \times \left([\pm a(s, \theta)^2 + b(s, \theta)^2] ds^2 + 2b(s, \theta) ds d\theta + d\theta^2 \right). \quad (74)$$

I. Rules 1 and 2 of the path integral geometry

Our goal is to constrain the functions $a(s, \theta)$, $b(s, \theta)$ and $\Omega(s, \theta)$ using rules 1 and 2 of Ref. [47], introduced as necessary conditions for assigning a *path integral* geometry to a tensor network.

Rule 1 of Ref. [47] (*compatibility with path integral*) states that the linear map implemented by an annulus $s \in [s_{\text{in}}, s_{\text{out}}]$ of such geometry, namely

$$V(s_{\text{in}}, s_{\text{out}}) \equiv \mathcal{P} \exp \left(- \int_{s_{\text{in}}}^{s_{\text{out}}} ds Q(s) \right), \quad (75)$$

where the generator reads (see Appendix (IV))

$$Q(s) \equiv \int_0^{2\pi} d\theta \left(a(s, \theta) h(\theta) - ib(s, \theta) p(\theta) \right) \quad (76)$$

for euclidean signature (+ sign) and

$$Q(s) \equiv \int_0^{2\pi} d\theta \left(ia(s, \theta) h(\theta) - ib(s, \theta) p(\theta) \right) \quad (77)$$

for lorentzian signature (− sign), should match, for $s_{\text{in}} = s_m$ and $s_{\text{out}} = s_{m+1}$, the linear map (71) implemented by the layer of euclidean MERA between spin chains m and $m + 1$, namely

$$\mathcal{W}_+^{(m, m+1)} \approx \exp \left(- \frac{2\pi}{N_0} q 2^m H_0 \right). \quad (78)$$

That is, $V(s_m, s_{m+1}) = \mathcal{W}_+^{(m, m+1)}$ or

$$\begin{aligned} \mathcal{P} \exp \left(- \int_{s_m}^{s_{m+1}} ds Q(s) \right) \\ = \exp \left(- \frac{2\pi}{N_0} q 2^m H_0 \right). \quad (\text{rule 1}) \end{aligned} \quad (79)$$

This results in a constraint on the signature (\pm sign) and the functions $a(s, \theta)$ and $b(s, \theta)$, but not on the scale factor $\Omega(s, \theta)$.

Rule 2 of Ref. [47] (*constant lattice spacing*) states that the proper distance between nearest neighbor sites (m, n) and $(m, n+1)$ in spin chain m is the same constant a_{UV} for all m and n . Then the length of the periodic spin chain m is $N_m a_{\text{UV}}$ and therefore its radius r_m is

$$r_m = \frac{N_m a_{\text{UV}}}{2\pi} = \frac{N_0 a_{\text{UV}}}{2\pi} 2^{-m} = r_0 e^{-m}, \quad (80)$$

$$r_0 \equiv \frac{N_0 a_{\text{UV}}}{2\pi}, \quad (81)$$

where r_0 is a reference radius.

In a constant s cut, the metric (74) reads $dl^2 = \Omega(s, \theta)^2 d\theta^2$ and therefore the distance (within the cut) between points $(s, m) = (s_m, \theta_{m,n})$ and $(s, m) = (s_m, \theta_{m,n+1})$ is

$$\int_{\theta_{m,n}}^{\theta_{m,n+1}} \sqrt{dl^2(s_m, \theta)} = \int_{\theta_{m,n}}^{\theta_{m,n+1}} d\theta \Omega(s_m, \theta). \quad (82)$$

Rule 2 then implies the constraint

$$\int_{\theta_{m,n}}^{\theta_{m,n+1}} d\theta \Omega(s_m, \theta) = a_{\text{UV}}. \quad (\text{rule 2}) \quad (83)$$

This is a constraint on the scale factor $\Omega(s, \theta)$, and not on the signature or functions $a(s, \theta)$ and $b(s, \theta)$ of metric (74).

There are now two possible routes to assigning a (path integral) geometry to the euclidean MERA. The first route simply identifies the metric H_2 with radius $R = a_{\text{UV}} q$ in the $r \gg R$ regime as one that satisfies rules 1 and 2. The second route first restricts the possible geometries on the grounds of discrete symmetries of the network. After that, requiring rules 1 and 2 is seen to completely specify the metric, which is again that of H_2 with radius $R = a_{\text{UV}} q$.

J. Path integral geometry of euclidean MERA on the circle

The first option is to provide an explicit example of a metric that fulfils rules 1 and 2. That is, to provide functions $a(s, \theta)$, $b(s, \theta)$ that lead to a generator $Q(s)$ compatible with rule 1 as expressed by condition (79), as well as to provide a scale factor $\Omega(s, \theta)$ compatible with rule 2 as expressed by condition (83).

One such example is given by

$$a(s, \theta) = \frac{a_{UV}}{r_0} q e^s, \quad b(s, \theta) = 0, \quad \Omega(s, \theta) = r_0 e^{-s}, \quad (84)$$

and the choice of euclidean signature (+ sign) in metric (74), which leads to the metric and generator

$$dl_{\mathcal{M}_+}^2 \equiv a_{UV}^2 q^2 ds^2 + r_0^2 e^{-2s} d\theta^2 \quad (85)$$

$$= r_0^2 e^{-2s} \left(\left(\frac{a_{UV}}{r_0} \right)^2 q^2 e^{2s} ds^2 + d\theta^2 \right), \quad (86)$$

$$Q_{\mathcal{M}_+} \equiv \frac{a_{UV}}{r_0} q e^s H_0. \quad (87)$$

Indeed, condition (79) for $Q(s) = Q_{\mathcal{M}_+}$ becomes

$$\exp \left(-\frac{a_{UV}}{r_0} q H_0 \int_{s_m}^{s_{m+1}} e^s ds \right) = \exp \left(-\frac{2\pi}{N_0} q 2^m H_0 \right) \quad (88)$$

which is fulfilled since

$$\int_{s_m}^{s_{m+1}} e^s ds = e^s \Big|_{2^m}^{2^{m+1}} = 2^m, \quad (89)$$

and (81) implies $a_{UV}/r_0 = 2\pi/N_0$, whereas condition (83) is fulfilled because

$$\int_{\theta_{m,n}}^{\theta_{m,n+1}} d\theta r_0 e^{-s} = r_0 e^{-s} \int_{\theta_{m,n}}^{\theta_{m,n+1}} d\theta = r_0 e^{-s} \frac{2\pi}{N_m} \quad (90)$$

$$= r_0 e^{-s} \frac{2\pi}{N_0} e^s = r_0 \frac{2\pi}{N_0} \quad (91)$$

$$= \frac{a_{UV} N_0}{2\pi} \frac{2\pi}{N_0} = a_{UV}. \quad (92)$$

We immediately recognize $dl_{\mathcal{M}_+}^2$ above as the metric $dl_{H_2}^2$ of the hyperbolic space H_2 with radius $R = a_{UV} q$, in the regime $r \gg R$, see Eq. (61). We also have

$$\frac{N_m}{2\pi q} = \frac{a_{UV} N_m}{2\pi a_{UV} q} = \frac{r_m}{R}, \quad (93)$$

so that indeed, the regime $r \gg R$ corresponds to $N_m \gg 2\pi q$ as anticipated earlier on.

K. First symmetries, then rules 1 and 2

Alternatively, we can start again with a general metric specified by three generic functions $a(s, \theta)$, $b(s, \theta)$, and $\Omega(s, \theta)$ in Eq. (74) and first impose rotation invariance and (apparent) scale invariance, then rules 1 and 2.

Rotation symmetry.— A layer $\mathcal{W}_+^{(m, m+1)}$ of euclidean MERA (between spin chains m and $m+1$) is a tensor network constructed by multiplying N_{m+1} times a basic building block in a way that it is explicitly invariant under rotations by an angle $\Delta\theta = 2\pi/N_{m+1} = 2\pi 2^{m+1}/N_0$, see Fig. 10(a). Notice that this *network* rotation invariance of the layer *implies* that the linear map implemented by the layer is rotation invariant. In addition, we may choose (as we do next) to interpret this *network*

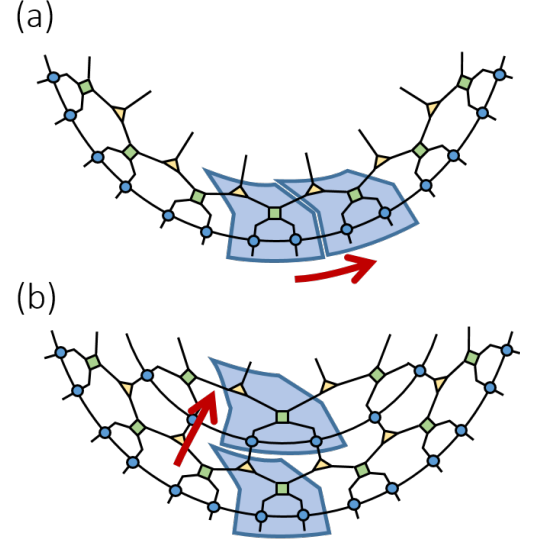


FIG. 10. (a) A layer of periodic euclidean MERA, obtained by multiplying a small unit cell of tensors, is invariant under discrete rotations. (b) Since each layer is made of copies of the same unit cell, there is also an apparent scale symmetry (or translation symmetry when moving in scale s).

rotation invariance as also implying that the distance between nearest neighbour spins is a constant $a_{UV, m}$ within each spin chain (which may still depend on the integer m that labels different spin chains).

We then *promote* the discrete rotation symmetry to continuous rotation symmetry of the metric,

$$a(s, \theta) \rightarrow a(s), \quad (94)$$

$$b(s, \theta) \rightarrow b(s), \quad (95)$$

$$\Omega(s, \theta) \rightarrow \Omega(s). \quad (96)$$

This promotion is compatible with, but not implied by, rules 1 and 2. It is an additional constraint on the metric, motivated by the discrete network rotation symmetry of \mathcal{W}_+ . We emphasize that layer $\mathcal{W}_+^{(m+1, m+2)}$ is only invariant under rotations by discrete angles $2\pi 2^{m+2}/N_0$, that is, by angles that are twice as large as those for layer $\mathcal{W}_+^{(m, m+1)}$. The euclidean MERA as a whole is then only invariant under rotations by the angles allowed by the discrete rotation symmetry of its top layer.

Scale symmetry.— The fact that all layers \mathcal{W}_+ of euclidean MERA are made from the same building block suggests an *apparent* symmetry of the network under simultaneous discrete rescaling in both the radial and angular directions,

$$s_m \rightarrow s_m + \log 2 = s_{m+1}, \quad (97)$$

$$\theta_{m,n} \rightarrow 2\theta_{m,n} = \theta_{m+1,n}, \quad (98)$$

see Fig. 10(b). This is an *apparent* (as opposed to actual) scale symmetry because it only applies in a local neighbourhood, as opposed to globally. Indeed, globally

the radius of the spin chain $m + 1$ is only half of the radius of the spin chain m . (On the Poincare patch, analyzed in Appendix II, the analogous rescaling will be a true discrete symmetry.) We can promote this (apparent) discrete scale symmetry to an (apparent) continuous scale symmetry by requiring that the metric be invariant under

$$s \rightarrow s + \log \lambda, \quad \theta \rightarrow \lambda \theta, \quad (99)$$

which implies

$$\Omega(s) = \Omega e^{-s}, \quad a(s) = a e^s, \quad b(s) = b e^s. \quad (100)$$

for arbitrary constants a, b, Ω .

In conclusion, imposing rotation and (apparent) scale symmetries we have arrived at the metric

$$dl^2 = \Omega^2 e^{-2s} ([\pm a^2 + b^2] e^{2s} ds^2 + 2b e^s ds d\theta + d\theta^2), \quad (101)$$

with unknown signature (\pm sign) and constants a, b , and Ω . This corresponds to a generator

$$Q(s) = e^s a \int d\theta h(\theta) - i e^s B \int d\theta p(\theta) \quad (102)$$

$$= e^s (aH - ibP) \quad (103)$$

for euclidean signature and

$$Q(s) = i e^s (aH - bP) \quad (104)$$

for lorentzian signature (see Appendix (IV)).

Imposing rule 1 we then obtain (i) euclidean signature (+ sign), (ii) $a = q(2\pi/N_0)$, and (iii) $b = 0$, whereas imposing rule 2 implies $\Omega = r_0$ and $a = q(a_{UV}/r_0)$. This uniquely leads to $dl_{\mathcal{M}_+}^2$ in Eq. (85), corresponding to H_2 with radius $R = a_{UV}q$ for $r \gg R$.

L. Regime $r \sim R$

Recall that the above geometric assignment is only valid when the size of the spin chain N_m is much larger than the width q of euclideanons in \mathcal{W}_+ or, equivalently, the radial coordinate r is much larger than the radius R . If our goal is for the tensor network to still be a discretized version of H_2 also for r on the order of the radius R , this can be accomplished by adjusting the width q_m of layer $\mathcal{W}_+^{(m,m+1)}$ of the tensor network as a function of m , so that the layer $\mathcal{W}_+^{(m,m+1)}$ implements a finite linear map as generated by Q_{H_2} in (52), instead of the asymptotic Q_{H_2} in (55).

M. Lorentzian signature: real time evolution on the circle

Next we study the linear map V obtained from a path integral on an annulus of de Sitter spacetime dS_2 and the tensor network geometry of the lorentzian MERA. The

analysis is very similar to the one above for hyperbolic space H_2 and the euclidean MERA. Accordingly, we proceed by only sketching the argument and highlighting the main differences with the previous case, to which we refer for further details.

As in Eq. (44), the linear map V is again defined in terms of a path integral on an annulus \mathcal{A} with boundaries at $r = r_{in}$ and $r = r_{out}$ (now for $r_{in}, r_{out} > a$) according to

$$\langle \varphi'(\theta) | V | \varphi(\theta) \rangle = \int [D\phi] e^{-iS[\phi(r,\theta)]}, \quad (105)$$

where now $S[\phi(r,\theta)]$ is the *lorentzian* action. For a diagonal metric of the form

$$dl^2 = \Omega(r)^2 (-a(r)^2 dr^2 + d\theta^2) \quad (106)$$

the generator Q of the linear map $V \approx \mathbb{1} - \epsilon Q$ for a thin cylinder is now given by

$$Q = ia(r) \int_0^{2\pi} d\theta h(\theta) = ia(r) H_0, \quad (107)$$

see Ref. [47] and Appendix (IV). Specifically, for de Sitter spacetime dS_2 in coordinates (r, θ) we have

$$a(r) = \frac{R}{r\sqrt{r^2 + R^2}} \quad (108)$$

Thus the metric and generator Q read:

$$dl_{dS_2}^2 = \frac{-R^2 dr^2}{r^2 - R^2} + r^2 d\theta^2 \quad (109)$$

$$= r^2 \left(\frac{-R^2 (dr/r)^2}{(r^2 - R^2)} + d\theta^2 \right), \quad (110)$$

$$Q_{dS_2} = i \frac{R}{r\sqrt{r^2 - R^2}} H_0, \quad (111)$$

with $r \geq R$. When the radial coordinate r is much larger than the radius R , $r \gg R$ (this is the regime where this geometry is more straightforwardly connected to the lorentzian MERA), the metric and generator simplify to

$$dl_{dS_2}^2 \approx \frac{-R^2 dr^2}{r^2} + r^2 d\theta^2 \quad (112)$$

$$= r^2 \left(\frac{-R^2 dr^2}{r^4} + d\theta^2 \right), \quad (113)$$

$$Q_{dS_2} \approx i \frac{R}{r^2} H_0, \quad (114)$$

and the path integral on a thick annulus $r \in [r_{in}, r_{out}]$ for $r_{in} \gg R$ corresponds to the finite linear map

$$V_{dS_2} = \mathcal{P} \exp \left(- \int_{r_{in}}^{r_{out}} dr Q_{dS_2} \right) \quad (115)$$

$$\approx \exp \left(-i H_0 \int_{r_{in}}^{r_{out}} \frac{R dr}{r^2} \right) \quad (116)$$

$$= \exp \left(-i \frac{R(r_{out} - r_{in})}{r_{out} r_{in}} H_0 \right). \quad (117)$$

We again introduce the scale radial coordinate $s \equiv \log(r_0/r)$, where r_0 is some reference radius with $r_0 \geq R$ such that the origin $s = 0$ of s corresponds to $r = r_0$. The metric of dS_2 , the generator Q_{dS_2} , and the finite gate V_{dS_2} read, in the simplifying regime $r \gg R$,

$$dl_{dS_2}^2 \approx -R^2 ds^2 + r_0^2 e^{-2s} d\theta^2 \quad (118)$$

$$= r_0^2 e^{-2s} \left(-\left(\frac{R}{r_0}\right)^2 e^{2s} ds^2 + d\theta^2 \right), \quad (119)$$

$$Q_{dS_2} \approx i \frac{R}{r_0} e^s H_0, \quad (120)$$

$$V_{dS_2} = \mathcal{P} \exp \left(- \int_{s_{\text{in}}}^{s_{\text{out}}} ds Q_{H_2} \right) \quad (121)$$

$$\approx \exp \left(-i \int_{s_{\text{in}}}^{s_{\text{out}}} ds \frac{a}{r_0} e^s H_0 \right) \quad (122)$$

$$= \exp \left(-i (e^{s_{\text{out}}} - e^{s_{\text{in}}}) \frac{R}{r_0} H_0 \right). \quad (123)$$

We note that the above two sets of expressions for Q_{dS_2} and V_{dS_2} , first in terms of the radial coordinate r and later in terms of the radial coordinate s , are mutually inconsistent. Indeed, in both cases we assume that time increases as we increase the radial coordinate: the first set assumes that time grows with r and the second set assumes that time grows with s . However, the radial coordinate r decreases as s increases, and therefore evolving forward in time s corresponds to evolving backwards in time r . From now on we follow the convention that time increases monotonically with s , that is, as the radial coordinate r decreases. The general formalism in Appendix (IV) assumes that time progresses when the time coordinate increases. Accordingly, we should correct Eqs. (111) and (114) for Q_{dS_2} by adding a minus sign, and Eqs. (116) and (117) for V_{dS_2} by removing the minus sign in the exponential. These expressions will not be used in the rest of this Appendix. (We chose to first write Eqs. (111), (114), (116), and (117) inconsistently, and then explain how to correct them, in order not to obscure their relation to the general formalism in Appendix (IV)).

Notice that in the euclidean signature case, addressed earlier on, the change in time direction does not affect the generator. This is because there the generator of time translations is Hermitian, not anti-Hermitian as in the lorentzian signature case. considerations would apply in the euclidean signature case. Indeed, in changing the orientation of the radial direction, we need to take the hermitian conjugate of the linear map. With lorentzian signature we have $V_{dS_2}(-\alpha) \equiv e^{-i\alpha H}$ for $\alpha \in \mathbb{R}$ and $H^\dagger = H$, and therefore $V_{dS_2}(\alpha)^\dagger = V_{dS_2}(-\alpha)$. Instead, with euclidean signature we have $V_{H_2}(\alpha) \equiv e^{-\alpha H}$ (again with $\alpha \in \mathbb{R}$ and $H^\dagger = H$) and thus $V_{H_2}(\alpha)^\dagger = V_{H_2}(\alpha)$.

A periodic layer \mathcal{W}_- of lorentzian MERA is made of q copies of the periodic lorentzian transfer matrix \mathcal{T}_- and a periodic layer \mathcal{W} of MERA,

$$\mathcal{W}_- \equiv \mathcal{W} (\mathcal{T}_-)^q. \quad (124)$$

The lorentzian transfer matrix \mathcal{T}_- is a tensor network, made of tensors called lorentzions, that acts on the Hilbert space of a periodic quantum spin chain made of N spins. By construction, it implements a real time evolution of the form

$$\mathcal{T}_- = \exp(-iH(N)) \approx \exp\left(i \frac{2\pi}{N} H_0\right). \quad (125)$$

Recall once more that the periodic layer \mathcal{W} maps low energy states on N spins to low energy states on $N/2$ spins as the identity operator $\mathbb{1}$. Therefore a periodic layer of lorentzian MERA implements the low energy linear map

$$\mathcal{W}_- \approx \exp\left(-iq \frac{2\pi}{N} H_0\right) = \exp\left(-iq \frac{a_{\text{UV}}}{r} H_0\right). \quad (126)$$

between states of the CFT from a circle of radius $r = Na_{\text{UV}}/2\pi$ to a smaller circle of radius $r/2$.

Given the discrete coordinates $(s_m, \theta_{m,n})$ from Eq. (73) applied now to label sites in the spin chains of a lorentzian MERA, and the candidate metric of Eq. (74), rule 1 implies

$$\mathcal{P} \exp\left(-i \int_{s_m}^{s_{m+1}} ds Q(s)\right) = \exp\left(-iq \frac{2\pi}{N_0} 2^m H_0\right). \quad (127)$$

whereas rule 2 implies Eq. (83) as in the euclidean MERA. Then the same choice of functions $a(s, \theta)$, $b(s, \theta)$, $\Omega(s, \theta)$ as in Eq. (84) as in the euclidean case, but with the choice of lorentzian signature ($-$ sign) in metric (74), leads to a solution of the constraints (127) (rule 1) and (83) (rule 2) with metric and generator

$$dl_{\mathcal{M}_-}^2 \equiv -a_{\text{UV}}^2 p^2 ds^2 + r_0^2 e^{-2s} d\theta^2 \quad (128)$$

$$= r_0^2 e^{-2s} \left(-\left(\frac{a_{\text{UV}}}{r_0}\right)^2 p^2 e^{2s} ds^2 + d\theta^2 \right), \quad (129)$$

$$Q_{\mathcal{M}_-} \equiv i \frac{a_{\text{UV}}}{r_0} q e^s H_0. \quad (130)$$

The metric corresponds to de Sitter spacetime dS_2 with radius $R = a_{\text{UV}} q$, see metric $dl_{dS_2}^2$ in Eq. (118).

N. Null signature: no time evolution on the circle

To compute the linear map V corresponding to a path integral on an annulus of the light cone L_2 , we will take the zero radius limit, $R \rightarrow 0$, of the derivation for either H_2 or dS_2 . We just list the resulting metric $dl_{L_2}^2$, generator Q_{L_2} , and linear map V_{L_2} ,

$$dl_{L_2}^2 = r^2 d\theta^2 = r_0^2 e^{-s} d\theta^2, \quad (131)$$

$$Q_{L_2} = 0, \quad (132)$$

$$V_{L_2} = \mathbb{1}, \quad (133)$$

as well as tensor network linear map \mathcal{W} and proposed tensor network geometry $dl_{\mathcal{M}}^2$

$$\mathcal{W} = \mathbb{1}, \quad (134)$$

$$dl_{\mathcal{M}}^2 = (r_0)^2 e^{-2s} d\theta^2. \quad (135)$$

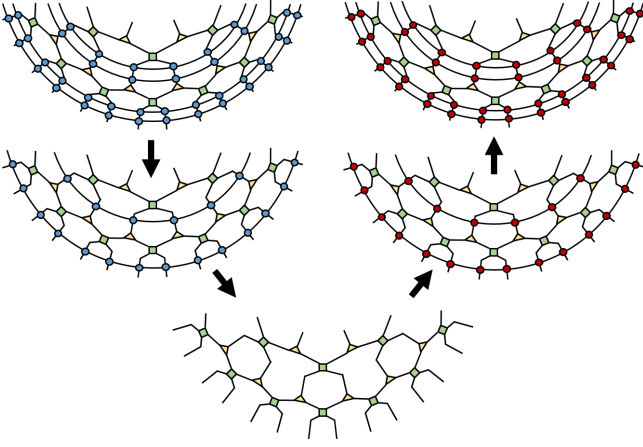


FIG. 11. We can consider a sequence of hyperbolic spaces H_2 for decreasing values of the (continuous) radius R , which has L_2 in the limit $R \rightarrow 0$, then continue with de Sitter spacetimes dS_2 for increasing values of the radius R , see Fig. 6. The above discrete sequence of tensor networks mimics that for discrete values $R = a_{UV}q$ of the radius R , for $q = 0, 1, 2, \dots$.

Since a layer \mathcal{W} of null MERA does not implement either euclidean nor lorentzian time evolution, from a path integral perspective the geometry of the null MERA is neither the hyperbolic space H_2 nor the de Sitter spacetime dS_2 .

O. Discrete sequence of tensor network geometries

To summarize, we have seen that the euclidean, and lorentzian MERA tensor networks correspond to a discrete version of a CFT path integral over the hyperbolic space H_2 and the de Sitter spacetime dS_2 in the $r \gg R$ regime, whereas the null MERA corresponds to a CFT path integral over the light cone L_2 . These three geometries can be embedded in the same ambient space $\mathbb{R}^{1,2}$, where both H_2 and dS_2 become L_2 in the limit of a small radius $R \rightarrow 0$. Analogously, the null MERA \mathcal{M} is a particular case of either the euclidean MERA \mathcal{M}_+ or lorentzian MERA \mathcal{M}_- , namely when there are $q = 0$ transfer matrices \mathcal{T} or \mathcal{T}_- (implementing euclidean or real time evolution) between layers \mathcal{W} , see Fig. 11.

II. APPENDIX: MERA ON THE REAL LINE

In this Appendix we review how to assign a path integral geometry to the *null*, *euclidean*, and *lorentzian* MERA on the real line, see Fig. 12. In this paper we denote L_2^p , H_2^p , and dS_2^p the light sheet, hyperbolic plane, and Poincare de Sitter spacetime geometries, respectively. Then the assignment of geometries to tensor networks is as follows:

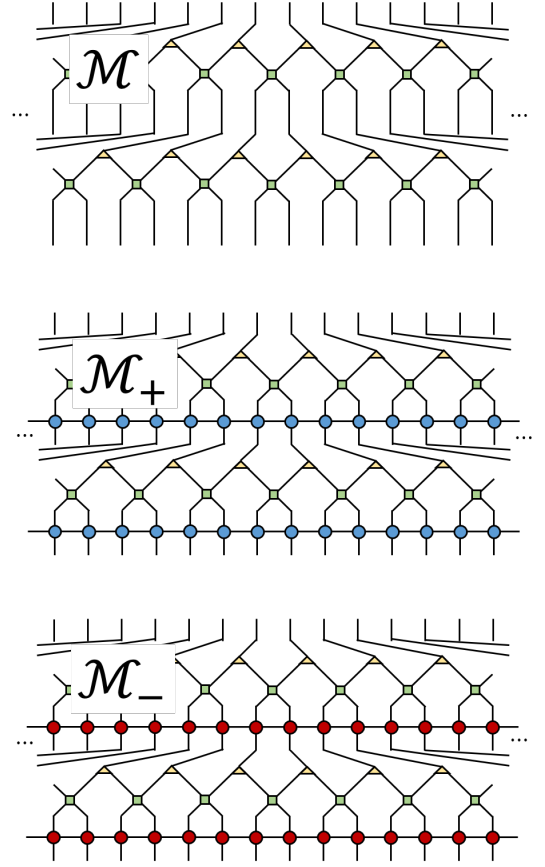


FIG. 12. Graphical representation of several MERA tensor networks on the line (only a finite part of two layers of each different MERA are displayed). Top: null MERA \mathcal{M} , with layers \mathcal{W} made of disentangers and isometries. Bottom left: euclidean MERA \mathcal{M}_+ , with layers $\mathcal{W}_+ = \mathcal{W}\mathcal{T}^q$ (for $q = 1$), where \mathcal{T} (made of euclidean transfer matrices, blue colour) is an euclidean transfer matrix that implements euclidean time evolution. Bottom right: lorentzian MERA \mathcal{M}_- , with layers $\mathcal{W}_- = \mathcal{W}\mathcal{T}_-^q$ (for $q = 1$), where \mathcal{T}_- (made of lorentzian transfer matrices, red colour) is a lorentzian transfer matrix that implements real time evolution.

null MERA \mathcal{M}	\leftrightarrow	light sheet L_2^p	
euclidean MERA \mathcal{M}_+	\leftrightarrow	hyperbolic plane H_2^p	(136)
lorentzian MERA \mathcal{M}_-	\leftrightarrow	Poincare de Sitter spacetime dS_2^p	

First we review how H_2^p , dS_2^p , and L_2^p can be embedded in a common three-dimensional ambient space, namely Poincare AdS_3 , denoted AdS_3^p . Then we characterize the different linear maps obtained through a CFT path integral on a strip of the H_2^p , dS_2^p , and L_2^p geometries. Finally, using the two rules of Ref. [47], we establish that an infinite layer of euclidean, lorentzian, and null MERA

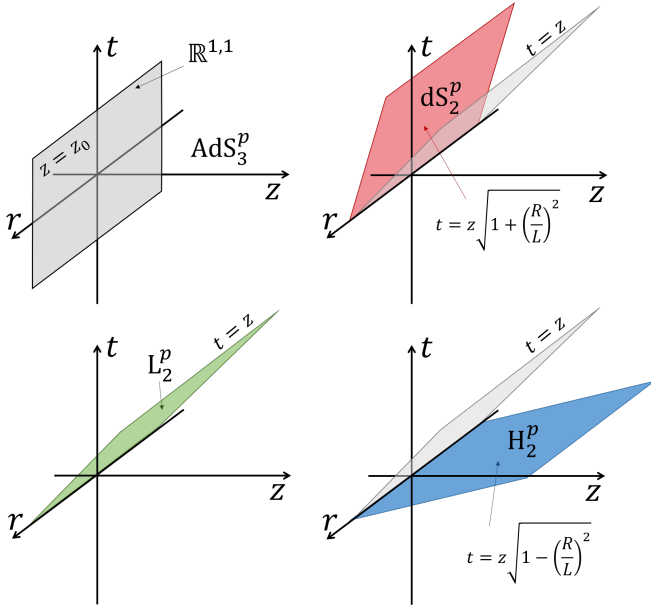


FIG. 13. Poincaré patch of anti de Sitter spacetime AdS_3 with radius L and coordinates (t, z, r) . For each fixed value of z we obtain a copy of Minkowski $\mathbb{R}^{1,1}$. By constraining t and z through $t = z\sqrt{1 + \sigma R^2/L^2}$ with $\sigma = +1, 0, -1$ we obtain the two-dimensional geometries H_2 , L_2 , and dS_2 , respectively.

corresponds to a strip of H_2^p , dS_2^p , and L_2^p geometries, respectively.

A. Embeddings in Poincaré anti de Sitter AdS_3^p

The Poincaré patch of AdS_3 with radius L has metric

$$dl_{\text{AdS}_3^p}^2 = \frac{-dt^2 + dz^2 + dr^2}{(z/L)^2} \quad (137)$$

for $r, t \in \mathbb{R}$ and $z \geq 0$. It is a useful ambient space for the three geometries under consideration, see Fig. 13. Indeed, each of the H_2^p , dS_2^p , and L_2^p geometries can be regarded as residing in an *upper half plane* (η, r) for $\eta > 0$, where η is some linear combination of time coordinate t and scale coordinate z . The euclidean, lorentzian, or null signature of the induced two-dimensional metric is determined by the ratio of time t versus scale z in this linear combination.

Firstly, a hyperbolic plane H_2^p with radius R , where $L \geq R > 0$, and metric

$$dl_{H_2^p}^2 = \frac{d\eta^2 + dr^2}{(\eta/R)^2} \quad (138)$$

can be obtained through the embedding

$$t = \sqrt{\left(\frac{L}{R}\right)^2 - 1} \eta, \quad z = \frac{L}{R} \eta \quad (139)$$

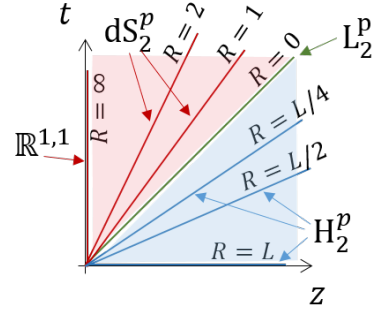


FIG. 14. The light sheet geometry L_2^p can be understood as the zero radius limit $R \rightarrow 0$ of both the hyperbolic plane H_2^p and Poincaré de Sitter space dS_2^p , as can be seen when considering these two-dimensional geometries as embedded in Poincaré AdS_3 , where t is the time coordinate, z is the (scale-)space coordinate, and the space coordinate r has been omitted.

for all r . Secondly, the (upper half plane) de Sitter space-time dS_2^p with radius $R > 0$ and metric

$$dl_{dS_2^p}^2 = \frac{-d\eta^2 + dr^2}{(\eta/R)^2} \quad (140)$$

is obtained through the embedding

$$t = \sqrt{\left(\frac{L}{R}\right)^2 + 1} \eta, \quad z = \frac{L}{R} \eta \quad (141)$$

for all r . (Notice that for $a = \infty$ we obtain $t = \eta$, $z = 0$ – that is, Minkowski $\mathbb{R}^{1,1}$). Finally, the light sheet L_2^p with metric

$$dl_{L_2^p}^2 = \frac{dr^2}{(\eta/R)^2} \quad (142)$$

is given by the embedding

$$t = \frac{L}{a} \eta, \quad z = \frac{L}{R} \eta \quad (143)$$

for all r , where $R > 0$ is here some (geometrically meaningless) constant that can be changed by rescaling η .

Recall that one merit of the Poincaré patch AdS_3^p of AdS_3 is that the metric (137) explicitly displays its invariance under a subgroup of symmetries of AdS_3 , namely the Poincaré group $SO(1,1)$ of transformations of the Minkowski space $\mathbb{R}^{1,1}$ obtained for each fixed value of the z coordinate, as coordinated by (t, r) and with metric $dl^2 \sim (-dt^2 + dr^2)$. However, the Poincaré patch AdS_3^p only covers part (that is, a patch) of AdS_3 .

In the subsequent discussion it is useful to parametrize these metrics using the scale coordinate z instead of η , where $z \geq 0$. In the above expressions we redefine $z \equiv \eta/R$ as a dimensionless coordinate (where now $R \geq 0$ is

not bounded by L) and obtain

$$dl_{H_2^p}^2 = \frac{R^2 dz^2 + dr^2}{z^2}, \quad (144)$$

$$dl_{dS_2^p}^2 = \frac{-R^2 dz^2 + dr^2}{z^2}, \quad (145)$$

$$dl_{L_2^p}^2 = \frac{dr^2}{z^2}. \quad (146)$$

These expressions make manifest that the metric of the light sheet L_2^p is the limit $R \rightarrow 0$ of either the metric of the hyperbolic plane H_2^p or of the Poincare de Sitter spacetime dS_2^p , see Fig. 14.

B. Linear map by path integral II: strip

The above geometries H_2^p , dS_2^p , and L_2^p can all be sliced into slices Σ_z defined by a constant value of the scale coordinate z . Each slice Σ_z corresponds to the real line. Two such real lines with scale coordinate $z = z_{\text{in}}$ and $z = z_{\text{out}}$, with $z_{\text{in}} < z_{\text{out}}$, define a horizontal strip \mathcal{S} characterized by $z \in [z_{\text{in}}, z_{\text{out}}]$, $r \in \mathbb{R}$, see Fig. 15(a).

Consider a two-dimensional CFT with field $\phi(z, r)$ and action functional $S[\phi(z, r)]$. In any of the three geometries, given Σ_{in} for $z = z_{\text{in}}$, we can define the Hilbert space $\mathcal{H}(\Sigma_{\text{in}})$ of the CFT on that real line in terms of basis states $|\varphi(r)\rangle$. Here $\varphi(r)$, for $r \in \mathbb{R}$, is a field configuration that results from restricting the field $\phi(z, r)$ to the line Σ_{in} . We can similarly define the Hilbert space $\mathcal{H}(\Sigma_{\text{out}})$ of the CFT on a second real line Σ_{out} given by $z = z_{\text{out}}$, again with basis $|\varphi(r)\rangle$. We can then identify the two Hilbert spaces \mathcal{H}_{in} and \mathcal{H}_{out} (from now on simply \mathcal{H}) by identifying basis vectors according to

$$|\varphi(r)\rangle_{\Sigma_{\text{in}}} \sim |\varphi'(r)\rangle_{\Sigma_{\text{out}}}, \text{ iff } \varphi(r) = \varphi'(r) \text{ for all } r. \quad (147)$$

For concreteness, from now on we continue the discussion for the hyperbolic plane H_2^p , and we postpone the analysis of dS_2^p and L_2^p until the end of this Appendix. Given a strip \mathcal{S} with boundaries Σ_{in} and Σ_{out} and the above identification between the corresponding Hilbert spaces, we introduce the linear map $\tilde{V} : \mathcal{H} \rightarrow \mathcal{H}$ given by the path integral on that strip \mathcal{S} , that is with matrix elements

$$\langle \varphi'(r) | \tilde{V} | \varphi(r) \rangle = \int [D\phi] e^{-S[\phi(z, r)]}, \quad (148)$$

where $S[\phi(z, r)]$ is the *euclidean* action of field configurations $\phi(z, r)$ restricted to the strip \mathcal{S} and with boundary conditions

$$\phi(z_{\text{in}}, r) = \varphi(r), \quad \phi(z_{\text{out}}, r) = \varphi'(r). \quad (149)$$

Above we denoted the linear map \tilde{V} instead of V because later on we will use V to denote a second linear map corresponding to a second set of coordinates (s, x) that are in some sense more natural when describing the euclidean MERA on the real line.

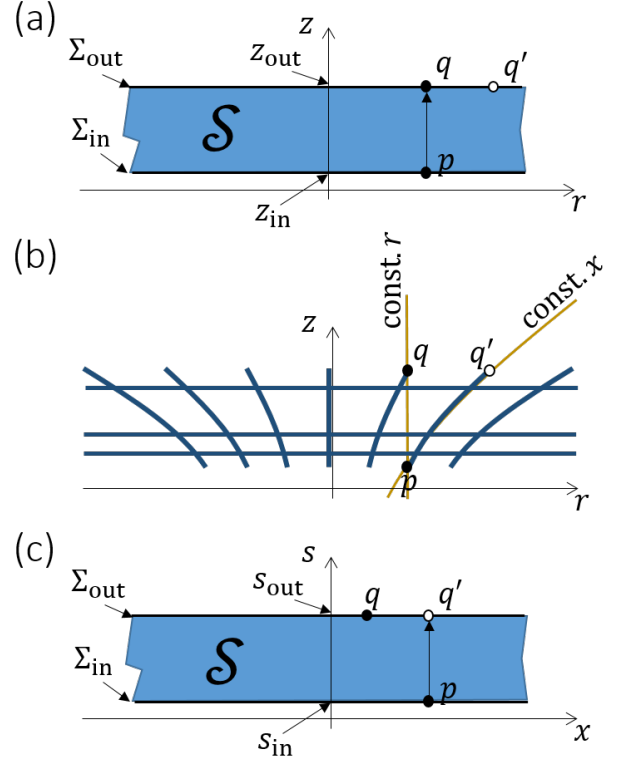


FIG. 15. (a) Strip \mathcal{S} with boundaries Σ_{in} and Σ_{out} corresponding to the lines $z = z_{\text{in}}$ and $z = z_{\text{out}}$ where $z_{\text{in}} < z_{\text{out}}$. The constant- r identification identifies point $p \in \Sigma_{\text{in}}$ with point $q \in \Sigma_{\text{out}}$. (b) Coordinates (s, x) as viewed in coordinates (z, r) . Notice that constant r and constant x curves are inequivalent. Therefore the constant- r and constant- x identifications of the boundaries of the strip \mathcal{S} are inequivalent. (c) The same strip \mathcal{S} with same boundaries Σ_{in} and Σ_{out} as above, now corresponding to the lines $s = s_{\text{in}}$ and $s = s_{\text{out}}$ where $s_{\text{in}} < s_{\text{out}}$ (where $s = \log(z)$). The constant- x identification identifies point $p \in \Sigma_{\text{in}}$ with point $q' \in \Sigma_{\text{out}}$.

C. Thin strip

In the limit of a thin annulus, when $z_{\text{out}} - z_{\text{in}} = \epsilon$ for small $\epsilon > 0$, we can expand the linear map $\tilde{V} \approx \mathbb{1} - \epsilon \tilde{Q}$ in terms of a generator \tilde{Q} . An expression for \tilde{Q} is found by specializing to the current case the general solution of Ref. [47], which is reviewed in Appendix (IV). For a diagonal metric of the form

$$dl^2 = \Omega(z)^2 (a(z)^2 dz^2 + dr^2) \quad (150)$$

this generator is

$$\tilde{Q} = a(z) \int_{-\infty}^{\infty} dr h(r) = a(z) H, \quad (151)$$

$$H \equiv \int_{-\infty}^{\infty} dr h(r). \quad (152)$$

For H_2^p in coordinates (z, r) we have a constant $a(z)$,

namely

$$a(z) = R, \quad (153)$$

$$(154)$$

and the metric and generator read:

$$dl_{\mathbb{H}_2^p}^2 = \frac{1}{z^2} (R^2 dz^2 + dr^2), \quad (155)$$

$$\tilde{Q}_{\mathbb{H}_2^p} = R H. \quad (156)$$

D. Thick strip

The path integral on a thick strip $z \in [z_{\text{in}}, z_{\text{out}}]$ produces the finite linear map

$$\tilde{V}_{\mathbb{H}_2^p} = \mathcal{P} \exp \left(- \int_{z_{\text{in}}}^{z_{\text{out}}} dz \tilde{Q}_{\mathbb{H}_2^p} \right) \quad (157)$$

$$= \exp \left(-RH \int_{z_{\text{in}}}^{z_{\text{out}}} dz \right) \quad (158)$$

$$= \exp(-R(z_{\text{out}} - z_{\text{in}})H). \quad (159)$$

corresponding to an euclidean time evolution by and amount $R(z_{\text{out}} - z_{\text{in}})$ of euclidean time.

E. Other coordinates

It is useful to also consider dimensionless coordinates (s, x) of the upper half plane given in terms of z and r according to (see Fig. 15(b))

$$s \equiv \log(z), \quad x \equiv \frac{r}{a_{\text{UV}} z}, \quad (160)$$

or

$$z = e^s, \quad r = a_{\text{UV}} e^s x, \quad (161)$$

where $s, x \in \mathbb{R}$ and a_{UV} is a short-distance length scale that will correspond to the lattice spacing in the tensor network. The metric of \mathbb{H}_2^p then reads

$$dl_{\mathbb{H}_2^p}^2 = a_{\text{UV}}^2 \left(\left[\frac{R^2}{a_{\text{UV}}^2} + x^2 \right] ds^2 + 2x ds dx + dx^2 \right). \quad (162)$$

In these coordinates the metric is no longer diagonal. Given two real lines Σ_{in} and Σ_{out} corresponding to $s = s_{\text{in}}$ and $s = s_{\text{out}}$, and corresponding Hilbert spaces \mathcal{H}_{in} and \mathcal{H}_{out} , a natural identification between states in \mathcal{H}_{in} and \mathcal{H}_{out} in the coordinates (s, x) is now (see Fig. 15(c))

$$|\varphi(x)\rangle_{\Sigma_{\text{in}}} \sim |\varphi'(x)\rangle_{\Sigma_{\text{out}}}, \quad \text{iff } \varphi(x) = \varphi'(x) \text{ for all } x, \quad (163)$$

which is not equivalent to that in Eq. (147). As a result, the linear map

$$\langle \varphi'(x) | V | \varphi(x) \rangle = \int [D\phi] e^{-S[\phi(s, x)]}, \quad (164)$$

where the boundary conditions of the field $\phi(s, x)$ are given by

$$\phi(s_{\text{in}}, x) = \varphi(x), \quad \phi(s_{\text{out}}, x) = \varphi'(x), \quad (165)$$

will have a different generator than $\tilde{V}_{\mathbb{H}_2^p}$ above. For a thin strip \mathcal{S} with $s_{\text{out}} - s_{\text{in}} = \epsilon$ for small $\epsilon > 0$, and metric

$$dl^2 = \Omega(s, x)^2 \times \quad (166)$$

$$([a(s, x)^2 + b(s, x)^2] ds^2 + 2b(s, x)^2 ds dx + dx^2) \quad (167)$$

the linear map $V \approx \mathbb{1} - \epsilon Q$ is generated by $Q = Q_0 - iQ_1$ (see Appendix (IV)) with

$$Q_0 \equiv \int_{\Sigma_{\text{in}}} dx a(s, x) h(x), \quad (168)$$

$$Q_1 \equiv \int_{\Sigma_{\text{in}}} dx b(s, x) p(x), \quad (169)$$

which for the current metric (162), with

$$\Omega(s, x) = a_{\text{UV}}, \quad a(s, x) = \frac{R}{a_{\text{UV}}}, \quad b(s, x) = x, \quad (170)$$

leads to

$$Q_0 \equiv \frac{R}{a_{\text{UV}}} \int_{\Sigma_{\text{in}}} dx h(x) = \frac{R}{a_{\text{UV}}} H, \quad (171)$$

$$Q_1 \equiv \int_{\Sigma_{\text{in}}} dx x p(x) = D, \quad (172)$$

that is

$$Q_{\mathbb{H}_2^p} = \frac{R}{a_{\text{UV}}} H - iD, \quad (173)$$

where H and D are the CFT Hamiltonian and dilation operators,

$$H \equiv \int_{-\infty}^{\infty} dx h(x), \quad D \equiv \int_{-\infty}^{\infty} dx x p(x). \quad (174)$$

The path integral on a finite strip $s \in [s_{\text{in}}, s_{\text{out}}]$, which corresponds to the strip $z \in [z_{\text{in}} = e^{s_{\text{in}}}, z_{\text{out}} = e^{s_{\text{out}}}]$, produces the linear map

$$V_{\mathbb{H}_2^p} = \mathcal{P} \exp \left(- \int_{s_{\text{in}}}^{s_{\text{out}}} ds Q_{\mathbb{H}_2^p} \right) \quad (175)$$

$$= \exp \left(- \left(\frac{R}{a_{\text{UV}}} H - iD \right) \int_{s_{\text{in}}}^{s_{\text{out}}} ds \right) \quad (176)$$

$$= \exp \left(-(s_{\text{out}} - s_{\text{in}}) \left(\frac{R}{a_{\text{UV}}} H - iD \right) \right). \quad (177)$$

The linear map $V_{\mathbb{H}_2^p}$ in Eq. (177) is not the same as $\tilde{V}_{\mathbb{H}_2^p}$ in Eq. (159), even though they are both produced by the path integral on the same strip, because they result from a different identification of the Hilbert space at the boundaries of the strip. To relate the two, we need to compensate for the difference in the identifications. Let

$$U(s) \equiv \exp(isD) \quad (178)$$

be the unitary transformation that applies a rescaling by a factor s . Then the two finite gates are related by

$$V_{H_2^p} = U(s_{\text{out}}) \tilde{V}_{H_2^p} U(s_{\text{in}})^\dagger \quad (179)$$

where $s_{\text{in}} \equiv \log z_{\text{in}}$, $s_{\text{out}} \equiv \log z_{\text{out}}$. In words, the gate $V_{H_2^p}$ is equivalent to $\tilde{V}_{H_2^p}$ after we compensate for two rescalings: one before and one after applying the gate, where these two rescalings are by a different amount, namely s_{in} and s_{out} .

Indeed, if we use that $i[D, H] = -H$, that is,

$$U(s) H U(s)^\dagger = e^{isD} H e^{-isD} = H e^{-s}, \quad (180)$$

$$U(s) e^{-\alpha H} U(s)^\dagger = \exp(-\alpha H e^{-s}) \quad (181)$$

then we first arrive to

$$e^{-\beta(\alpha H - iD)} = \left(e^{-\epsilon(\alpha H - iD)} \right)^N \quad (182)$$

$$\approx (e^{-\epsilon\alpha H} e^{i\epsilon D}) (e^{-\epsilon\alpha H} e^{i\epsilon D}) \dots (e^{-\epsilon\alpha H} e^{i\epsilon D}) \quad (183)$$

$$= e^{-\epsilon\alpha H} (e^{i\epsilon D} e^{-\epsilon\alpha H} e^{-i\epsilon D}) (e^{i2\epsilon D} e^{-\epsilon\alpha H} e^{-i2\epsilon D}) \quad (184)$$

$$\dots \times (e^{i(N-1)\epsilon D} e^{-\epsilon\alpha H} e^{-i(N-1)\epsilon D}) e^{iN\epsilon D} \quad (185)$$

$$= \exp(-\epsilon\alpha H) \exp(-\epsilon\alpha e^{-\epsilon} H) \exp(-\epsilon\alpha e^{-2\epsilon} H) \quad (186)$$

$$\dots \times \exp(-\epsilon\alpha e^{-(N-1)\epsilon} H) e^{iN\epsilon D} \quad (187)$$

$$= \exp\left(-\epsilon\alpha \left(1 + e^{-\epsilon} + \dots + e^{-(N-1)\epsilon}\right) H\right) e^{i\beta D} \quad (188)$$

$$= e^{-\mu H} e^{i\beta D}, \quad (189)$$

where $\epsilon \equiv \beta/N$ and where, in the limit $\epsilon \rightarrow 0$,

$$\mu = \alpha \lim_{\epsilon \rightarrow 0} \sum_{n=0}^{N-1} \epsilon e^{-\epsilon n} \quad (190)$$

$$= \alpha \int_0^\beta d\beta' e^{-\beta'} = \alpha (1 - e^{-\beta}). \quad (191)$$

Similarly, we can find

$$e^{-\beta(\alpha H - iD)} = e^{i\beta D} e^{-\mu' H} \quad (192)$$

with

$$\mu' = \alpha \lim_{\epsilon \rightarrow 0} \sum_{n=0}^{N-1} \epsilon e^{\epsilon n} \quad (193)$$

$$= \alpha \int_0^\beta d\beta' e^{\beta'} = \alpha (e^\beta - 1). \quad (194)$$

Thus, we have seen that

$$e^{-\alpha(1-e^{-\beta})H} e^{i\beta D} = e^{-\beta(\alpha H - iD)} = e^{i\beta D} e^{-\alpha(e^\beta - 1)H}. \quad (195)$$

Then, returning to Eq. (179), we see that, for $\Delta s \equiv$

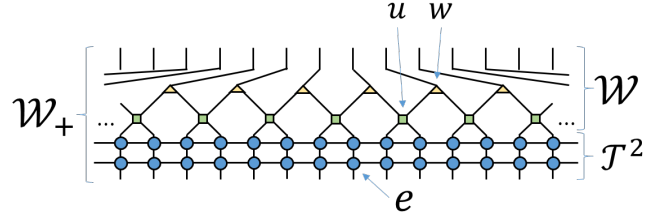


FIG. 16. Layer \mathcal{W}_+ of euclidean MERA on the line. Only part of this infinite layer is shown. \mathcal{W}_+ is made of the product of q euclidean transfer matrices \mathcal{T} ($q = 2$ in the figure) and a layer \mathcal{W} of null or regular MERA, see Eq. (201). Each euclidean transfer matrix \mathcal{T} consist of a one-dimensional array of tensors e called euclideanons. Each layer \mathcal{W} of null MERA is made of tensors u and w called disentanglers and isometries.

$s_{\text{out}} - s_{\text{in}}$, as announced above we have

$$V_{H_2^p} = e^{-\Delta s(\alpha H - iD)} = e^{i\Delta s D} e^{-\alpha(e^{\Delta s} - 1)H} \quad (196)$$

$$= e^{i\Delta s D} U(s_{\text{in}})^\dagger \left(U(s_{\text{in}}) e^{-\alpha(e^{\Delta s} - 1)H} U(s_{\text{in}}) \right) U(s_{\text{in}})^\dagger$$

$$= U(s_{\text{out}}) \exp(-\alpha(e^{\Delta s} - 1)e^{s_{\text{in}}H}) U(s_{\text{in}})^\dagger \quad (197)$$

$$= U(s_{\text{out}}) \exp(-\alpha(e^{s_{\text{out}}} - e^{s_{\text{in}}})H) U(s_{\text{in}})^\dagger \quad (198)$$

$$= U(s_{\text{out}}) \exp(-\alpha(z_{\text{out}} - z_{\text{in}})H) U(s_{\text{in}})^\dagger \quad (199)$$

$$= U(s_{\text{out}}) \tilde{V}_{H_2^p} U(s_{\text{in}})^\dagger. \quad (200)$$

where we used α for R/a_{UV} to simplify the notation.

F. Linear map of \mathcal{W}_+ on the line

A layer \mathcal{W}_+ on the line is made of the product of q euclidean transfer matrices \mathcal{T} followed by a layer \mathcal{W} of null MERA,

$$\mathcal{W}_+ \equiv \mathcal{W} \mathcal{T}^q, \quad (201)$$

see Fig. 16.

Each euclidean transfer matrix \mathcal{T} is made of an infinite row of euclideanons and, by construction, implements the euclidean time evolution

$$\mathcal{T} \approx e^{-H}, \quad (202)$$

where the spin Hamiltonian H reads

$$H \equiv \sum_{l=-\infty}^{\infty} h_l. \quad (203)$$

On the other hand, which transformation a layer \mathcal{W} of null MERA on the real line implements depends on how we identify the Hilbert spaces of the two spin chains it connects. Following with the above discussion in the continuum, we consider two natural identifications, given by keeping either r or x constant. The constant- r identification in the line is analogous to the constant- θ identification in the circle discussed in Appendix I. Pairs of

contiguous sites in the lower spin chain are mapped into single sites of the upper spin chain. We can then export the result from the circle to the line and conclude that \mathcal{W} (denoted $\tilde{\mathcal{W}}$ in what follows) acts as the identity $\mathbb{1}$ on CFT states on the line,

$$\tilde{\mathcal{W}} \approx \mathbb{1} \quad (\text{constant-}r \text{ identification}). \quad (204)$$

In turn, in the constant- x identification, which we will follow here, we identify each spin on the lower spin chain with a spin in the upper spin chain. (This was not possible in the circle because the lower spin chain had twice as many spins as the upper spin chain, but on the line this is not a problem, given that each spin chain has infinitely many spins.) The constant- x identification has been used implicitly in the literature e.g. when extracting conformal data from the scale invariant MERA, in that the identification of local scaling operators is based on diagonalizing a local scaling superoperator that identifies a small number (e.g. three) of sites in one spin chain with the same number of sites in the other spin chain. In this context, a layer of MERA implements a change of scale by a factor $1/2$, that is

$$\mathcal{W} \approx 2^{iD} = \exp(i \log(2)D) \quad (\text{const.-}x \text{ ident.}). \quad (205)$$

Accordingly, the linear map implemented by a layer of euclidean MERA on the line is now:

$$\mathcal{W}_+ \approx 2^{iD} e^{-qH} = 2^{-(qH-iD)}, \quad (206)$$

where we used Eq. (195) specialize to $\beta = \log 2$ to obtain

$$e^{-\frac{\alpha}{2}H} 2^{iD} = 2^{-(\alpha H-iD)} = 2^{iD} e^{-\alpha H}. \quad (207)$$

G. Discrete coordinates on the euclidean MERA on the line

Consider the euclidean MERA on the line. We use an integer m to label each infinite spin chain between two layers of the euclidean MERA. Each site in spin chain m is labelled by a pair (m, n) of integers, see Fig. 17(a). We then associate the discrete coordinates $(s_m, x_{m,n})$ to site (m, n) according to

$$s_m = m \log 2, \quad x_{m,n} = n + \frac{1}{2}, \quad (208)$$

where a_{UV} is a length scale, see Fig. 17(b). Notice that both s_m and $x_{m,n}$ are dimensionless.

A candidate geometry for the euclidean MERA is given by a generic metric in the continuous coordinates (s, x) (see Appendix (IV)),

$$dl^2 = \Omega(s, x)^2 \times ([\pm a(s, x)^2 + b(s, x)^2] ds^2 + 2b(s, x)^2 ds dx + dx^2) \quad (209)$$

where again both s and x are dimensionless, as are functions $a(s, x)$ and $b(s, x)$, whereas the local scale factor $\Omega(s, x)$ has dimensions of length.

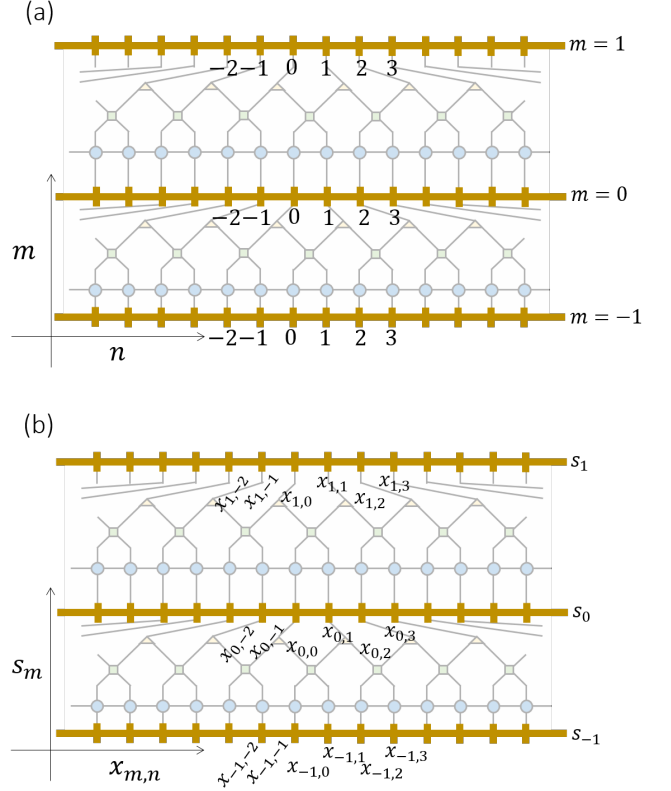


FIG. 17. (a) We label each spin chain between two layers of euclidean MERA by an integer m , and each sites within that spin chain by the pair (m, n) . (b) We then assign to site (m, n) discrete coordinates $(s_m, x_{m,n})$ as given in (208).

H. Rules 1 and 2 of path integral geometry

Our goal is to determine the signature (\pm sign) and the functions $a(s, x)$, $b(s, x)$, $\Omega(s, x)$ using rules 1 and 2 of Ref. [47].

Rule 1 of Ref. [47] (*compatibility with path integral*) states that the linear map implemented by a strip $s \in [s_{\text{in}}, s_{\text{out}}]$ of such geometry, namely

$$V(s_{\text{in}}, s_{\text{out}}) \equiv \mathcal{P} \exp \left(- \int_{s_{\text{in}}}^{s_{\text{out}}} ds Q(s) \right) \quad (210)$$

where the generator reads

$$Q(s) = \int_{-\infty}^{\infty} dx \left(a(s, x) h(x) - ib(s, x) p(x) \right) \quad (211)$$

for euclidean signature (+ sign) and

$$Q(s) = \int_{-\infty}^{\infty} dx \left(ia(s, x) h(x) - ib(s, x) p(x) \right) \quad (212)$$

for lorentzian signature ($-$ sign), should match, for $s_{\text{in}} = s_m$ and $s_{\text{out}} = s_{m+1}$, the linear map (206) implemented by the layer $\mathcal{W}_+^{(m, m+1)}$ of euclidean MERA between spin

chains m and $m+1$. That is, $V(s_m, s_{m+1}) = \mathcal{W}_+^{(m, m+1)}$ or

$$\mathcal{P} \exp \left(- \int_{s_m}^{s_{m+1}} ds Q(s) \right) = 2^{-(qH - iD)}. \quad (213)$$

This is a constraint on the functions $a(s, x)$ and $b(s, x)$ and the choice of signature (\pm sign), but not on the scale factor $\Omega(s, x)$.

Rule 2 of Ref. [47] (*constant lattice spacing*) states that the proper distance between nearest neighbor sites (m, n) and $(m, n+1)$ in spin chain m is the same constant a_{UV} for all m and n . In a constant s cut, the metric (209) reads $dl^2 = \Omega(s, x)^2 dr^2$ and therefore the distance (within the cut) between points $(s_m, x_{m,n})$ and $(s_m, x_{m,n+1})$ is

$$\int_{x_{m,n}}^{x_{m,n+1}} \sqrt{dl^2(s_m, x)} = \int_{x_{m,n}}^{x_{m,n+1}} dx \Omega(s_m, x). \quad (214)$$

Rule 2 then implies the constraint

$$\int_{x_{m,n}}^{x_{m,n+1}} dx \Omega(s_m, r) = a_{UV}. \quad (215)$$

This is a constraint on the scale factor $\Omega(s, x)$, and not on the signature or functions $a(s, x)$ and $b(s, x)$ of metric (209).

There are now two possible routes to assigning a (path integral) geometry to the euclidean MERA. The first route simply identifies the metric H_2 with radius $R = a_{UV}q$ as one that satisfies rules 1 and 2. The second route first restricts the possible geometries on the grounds of discrete symmetries of the network. After that, requiring rules 1 and 2 is seen to completely specify the metric, which is again that of H_2 with radius $R = a_{UV}q$.

I. Path integral geometry of euclidean MERA on the line

Consider the following functions

$$a(s, x) = q, \quad b(s, x) = x, \quad \Omega(s, x) = a_{UV}, \quad (216)$$

and the choice of euclidean signature (+ sign) in metric (209). They produce the metric and generator

$$dl_{\mathcal{M}_+^p}^2 \equiv a_{UV}^2 ([q^2 + x^2] ds^2 + 2x ds dx + dx^2) \quad (217)$$

$$Q_{\mathcal{M}_+^p} \equiv qH - iD \quad (218)$$

which fulfil rules 1 and 2.

Indeed, condition (213) is fulfilled since we find

$$- \int_{s_m}^{s_{m+1}} ds Q_{\mathcal{M}_+^p} = -(s_{m+1} - s_m)(qH - iD) \quad (219)$$

$$= -\log 2 (qH - iD), \quad (220)$$

whereas condition (215) is fulfilled because

$$\int_{x_{m,n}}^{x_{m,n+1}} dx a_{UV} = a_{UV}(x_{m,n+1} - x_{m,n}) = a_{UV}. \quad (221)$$

We immediately recognize $dl_{\mathcal{M}_+^p}^2$ above as the metric (162) of the hyperbolic plane H_2^p with radius $R = qa_{UV}$. In the coordinates (z, r) it reads

$$dl_{\mathcal{M}_+^p}^2 = \frac{1}{z^2} ((qa_{UV})^2 dz^2 + dr^2). \quad (222)$$

J. First symmetries, then rules 1 and 2

Alternatively, we can start again with a general metric specified by a choice of signature and three generic functions $a(s, x)$, $b(s, x)$, and $\Omega(s, x)$ in Eq. (209) and first impose translation and scale invariance, then rules 1 and 2.

Translation symmetry.— A layer $\mathcal{W}_+^{(m, m+1)}$ is a tensor network constructed as the infinite product of a basic building block in a way that it is explicitly invariant under discrete translations. Specifically, under translations by one site of the spin chain $m+1$ or, equivalently, two sites of the spin chain m , see Fig. 18(a). This *network* translation invariance of the layer *implies* that the linear map implemented by the layer is also translation invariant. In addition, we may choose (as we do next) to interpret this *network* translation invariance of each layer of euclidean MERA as also implying that the distance between nearest neighbour spins is a constant $a_{UV, m}$ within each spin chain, which may still depend on the integer m that labels different spin chains. The translation symmetry of k layers is limited to translations by one site of the spin chain placed above the top layer. Let this top spin chain have label 0, and let $m \in [0, k]$. The network is invariant under the discrete transformation

$$s_m \rightarrow s_m, \quad x_{m,n} \rightarrow x_{m,n} + 2^{-m} = x_{m,n} + e^{-s_m}. \quad (223)$$

We then *promote* the discrete translation symmetry to continuous translation symmetry of the metric, by demanding that it be invariant under

$$s \rightarrow s, \quad x \rightarrow x + \lambda e^{-s} \quad (224)$$

for an infinitesimal λ .

Scale symmetry.— The fact that all layers \mathcal{W}_+ of euclidean MERA are identical to each other, implies a second discrete symmetry of the network, namely discrete scale transformations, see Fig. 18(b). Indeed, consider the shift

$$s_m \rightarrow s_m + \log 2 = s_{m+1}, \quad (225)$$

$$x_{m,n} \rightarrow x_{m,n} = x_{m+1,n}. \quad (226)$$

As we did above with translation invariance, we can now *promote* this discrete scale symmetry of the network to a continuous scale symmetry of the continuous metric by requiring that it be invariant under the transformation

$$s \rightarrow s + \log \lambda, \quad x \rightarrow x, \quad (227)$$

for an infinitesimally small λ .

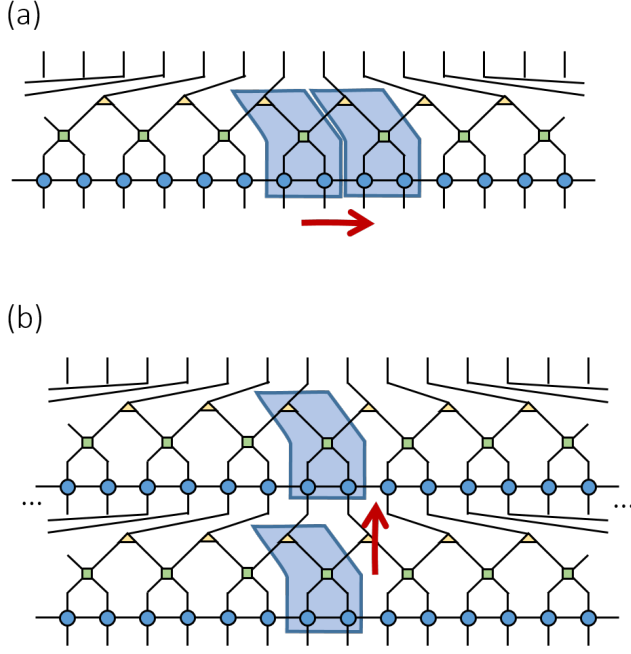


FIG. 18. (a) A layer of euclidean MERA on the line, obtained by multiplying a small unit cell of tensors, is invariant under discrete translations. (b) Since each layer of euclidean MERA is identical, the network is invariant under discrete scale transformations.

We emphasize that these promotions of discrete network symmetries to continuous symmetries can be seen to be compatible with, but are not implied by, rules 1 and 2. It is a way of further restricting the metric. One could consider adding a rule 3 that says that in the presence of a discrete network symmetry, the continuous metric should also have a suitable continuous version of that symmetry. A problem with proceeding this way is that a discrete symmetry does not determine a continuous symmetry uniquely, so such rule 3 would be ambiguous and still require that the discrete network symmetry be promoted to some preferred choice of continuous symmetry.

To enforce the above two symmetries on the metric, it is convenient to use the fact that they correspond to translations $(z, r) \rightarrow (z, r + \lambda)$ and to rescaling $(z, r) \rightarrow \lambda(z, r)$ in the coordinates (z, r) , to produce

$$dl^2 = \frac{C^2}{z^2} ([\pm A^2 + B^2] dz^2 + 2Bdzdr + dr^2), \quad (228)$$

which in the (s, x) coordinates corresponds to

$$a = \frac{A}{a_{UV}}, \quad b = x + \frac{B}{a_{UV}}, \quad \Omega = a_{UV}C, \quad (229)$$

that is

$$dl^2 = C^2 a_{UV}^2 \left(\left[\pm \frac{A^2}{a_{UV}^2} + \left(x + \frac{B}{a_{UV}} \right)^2 \right] ds^2 \right. \quad (230)$$

$$\left. + 2 \left(x + \frac{B}{a_{UV}} \right) dsdx + dx^2 \right), \quad (231)$$

with unknown signature (\pm sign) and constants A , B , and C .

Imposing rule 1 through constraint (213) we then obtain euclidean signature (sign $+$), and the values $A = a_{UV}q$ and $B = 0$. Moreover, imposing rule 2 through constraint (215) we obtain $C = 1$. This uniquely leads to $dl_{\mathcal{M}_+^p}^2$ in Eq. (217), corresponding to the H_2^p metric in (162) with radius $R = a_{UV}q$.

K. Relation to previous derivations

Our second derivation of a continuous metric for the euclidean MERA on the line, based on symmetries, is similar but not equivalent to previous derivations of a continuous metric for the null MERA [15–18].

Arguing in terms of symmetries alone (including that the lattice spacing a_{UV} is constant throughout the network) we already arrive at a metric

$$dl^2 = \left(\frac{a_{UV}}{z} \right)^2 ([\pm A^2 + B^2] dz^2 + 2Bdzdr + dr^2), \quad (232)$$

for unknown signature (sign \pm) and constants A, B . In order to determine the signature and set $B = 0$ (that is, to recover the metric of H_2^p) and to further relate A to q/a_{UV} (that is, to establish that that the radius R of H_2^p is equal to $a_{UV}q$) we require rule 1.

As mentioned above, H_2^p , dS_2^p , and L_2^p have in common the symmetry group they inherit from AdS_3^p , which includes both translations and rescalings. Reasoning in terms of symmetries only (that is, without rule 1) we can attach any of the above geometries to the euclidean MERA. Therefore we conclude that rule 1 (or some other rule that goes beyond symmetry considerations) is essential in order to decide which of these three geometries should be assigned to the euclidean MERA.

L. Lorentzian signature: time evolution on the line

Next we study the linear map V obtained from a path integral on a strip of Poincare de Sitter spacetime dS_2^p and the tensor network geometry of the lorentzian MERA on the line. The analysis is very similar to the one above for hyperbolic space H_2^p and the euclidean MERA, and therefore we will proceed by sketching the argument and highlighting the differences with the previous case, to which we refer for further details.

As in Eq. (233), the linear map \tilde{V} is again defined in terms of a path integral on a strip \mathcal{S} with boundaries at $z = z_{\text{in}}$ and $z = z_{\text{out}}$ according to

$$\langle \varphi'(r) | \tilde{V} | \varphi(r) \rangle = \int [D\phi] e^{-iS[\phi(z, r)]}, \quad (233)$$

where now $S[\phi(z, r)]$ is the *lorentzian* action. For a thin strip, the linear map reads $\tilde{V} \approx \mathbb{1} - \epsilon \tilde{Q}$. For a diagonal

metric of the form

$$dl^2 = \Omega(z)^2 (-a(z)^2 dz^2 + dr^2) \quad (234)$$

this generator is

$$\tilde{Q} = ia(z) \int_{-\infty}^{\infty} dr h(r) = ia(z) H, \quad (235)$$

$$H \equiv \int_{-\infty}^{\infty} dr h(r). \quad (236)$$

For dS_2^p in coordinates (z, r) we have a constant $a(z)$, namely

$$a(z) = R, \quad (237)$$

$$(238)$$

and the metric and generator read:

$$dl_{dS_2^p}^2 = \frac{1}{z^2} (-R^2 dz^2 + dr^2), \quad (239)$$

$$\tilde{Q}_{dS_2^p} = iR H. \quad (240)$$

The path integral on a thick strip $z \in [z_{\text{in}}, z_{\text{out}}]$ then produces the finite linear map

$$\tilde{V}_{dS_2^p} = \mathcal{P} \exp \left(- \int_{z_{\text{in}}}^{z_{\text{out}}} dz \tilde{Q}_{dS_2^p} \right) \quad (241)$$

$$= \exp \left(-iRH \int_{z_{\text{in}}}^{z_{\text{out}}} dr \right) \quad (242)$$

$$= \exp (-iR (z_{\text{out}} - z_{\text{in}}) H). \quad (243)$$

corresponding to a real time evolution by an amount $R(z_{\text{out}} - z_{\text{in}})$ of time. In terms of the dimensionless coordinates (s, x) , with $s = \log(z)$ and $x = r/(a_{\text{UV}} z)$, the metric of dS_2^p is no longer diagonal and reads

$$dl_{dS_2^p}^2 = a_{\text{UV}}^2 \left(\left[\frac{-R^2}{a_{\text{UV}}^2} + x^2 \right] ds^2 + 2x ds dx + dx^2 \right). \quad (244)$$

With the constant- x identification of Hilbert spaces at the boundaries of the strip, see Eq. (163), the linear map

$$\langle \varphi'(x) | V | \varphi(x) \rangle = \int [D\phi] e^{-iS[\phi(s, x)]}, \quad (245)$$

for a thin strip ($z_{\text{out}} - z_{\text{in}} \equiv \epsilon \ll 1$) decomposes as $V \approx \mathbb{1} - \epsilon Q$ with generator $Q = iQ_0 - iQ_1$ for Q_0 and Q_1 given by Eqs. (171)-(172), so that

$$Q_{dS_2^p} = i \left(\frac{R}{a_{\text{UV}}} H - D \right), \quad (246)$$

$$V_{dS_2^p} = \mathcal{P} \exp \left(- \int_{s_{\text{in}}}^{s_{\text{out}}} ds Q_{dS_2^p} \right) \quad (247)$$

$$= \exp \left(-i(s_{\text{out}} - s_{\text{in}}) \left(\frac{R}{a_{\text{UV}}} H - D \right) \right), \quad (248)$$

where (compare with Eq. (179))

$$V_{dS_2^p} = U(s_{\text{out}}) \tilde{V}_{dS_2^p} U(s_{\text{in}})^\dagger. \quad (249)$$

A layer \mathcal{W}_- of lorentzian MERA on the line is made of the product of q lorentzian transfer matrices \mathcal{T}_- (each of which has been built to implement a real time evolution $\mathcal{T}_- \approx e^{-iH}$) followed by a layer \mathcal{W} of null MERA,

$$\mathcal{W}_- \equiv \mathcal{W} \mathcal{T}_-^q, \quad (250)$$

and implements the linear map

$$\mathcal{W}_- \approx 2^{iD} e^{iqH} = 2^{-i(qH-D)}. \quad (251)$$

Given the discrete coordinates $(s_m, x_{m,n})$ from Eq. (208) applied now to label sites in the spin chains of a lorentzian MERA, and the candidate metric of Eq. (209), rule 1 implies

$$\mathcal{P} \exp \left(- \int_{s_m}^{s_{m+1}} ds Q(s) \right) = 2^{-i(qH+D)}. \quad (252)$$

whereas rule 2 implies Eq. (215) as in the euclidean MERA. Then the same choice of functions $a(s, x)$, $b(s, x)$ and $\Omega(s, x)$ as in Eq. (216) from the euclidean signature case, but with the choice of a lorentzian signature ($-$ sign) in the metric (209), leads to a solution of the constraints (252) (rule 1) and (215) with metric and generator

$$dl_{\mathcal{M}_-^p}^2 \equiv a_{\text{UV}}^2 ([-q^2 + x^2] ds^2 + 2x ds dx + dx^2) \quad (253)$$

$$Q_{\mathcal{M}_-^p} \equiv -i(qH - D). \quad (254)$$

The metric corresponds to Poincare de Sitter spacetime dS_2^p with radius $R = a_{\text{UV}} q$. The same conclusion is reached by first imposing translation and scale invariance (exactly in the same way as in the case of euclidean signature) and then enforce rules 1 and 2.

M. Null signature: no time evolution on the line

To compute the linear maps corresponding to a path integral on a strip of the light sheet geometry L_2^p we will take the zero radius limit, $R \rightarrow 0$, of the derivation for either H_2^p or dS_2^p . We just list the resulting objects. In the coordinates (z, r) the metric $dl_{L_2^p}^2$, generator $\tilde{Q}_{L_2^p}$, and linear map $\tilde{V}_{L_2^p}$ read

$$dl_{L_2^p}^2 = \frac{dr^2}{z^2}, \quad (255)$$

$$\tilde{Q}_{L_2^p} = 0, \quad (256)$$

$$\tilde{V}_{L_2^p} = \mathbb{1}. \quad (257)$$

In the coordinates (s, x) the metric $dl_{L_2^p}^2$, generator $Q_{L_2^p}$, and linear map $V_{L_2^p}$ read

$$dl_{L_2^p}^2 = a_{\text{UV}}^2 (x^2 ds^2 + 2x ds dx + dx^2), \quad (258)$$

$$Q_{L_2^p} = -iD, \quad (259)$$

$$V_{L_2^p}(s_{\text{in}}, s_{\text{out}}) = e^{i(s_{\text{out}} - s_{\text{in}})D}. \quad (260)$$

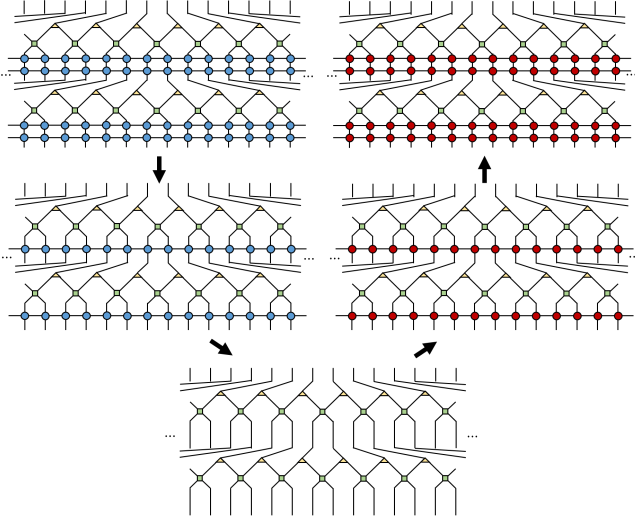


FIG. 19. We can consider a sequence of hyperbolic planes H_2^p for decreasing values of the (continuous) radius R , which has the light sheet L_2^p as its $R \rightarrow 0$ limit, then continue with Poincare de Sitter spacetimes dS_2^p for increasing values of the radius R , see Fig. 14. The above discrete sequence of tensor networks mimics that for discrete values $R = a_{UV}q$ of the radius R , for $q = 0, 1, 2, \dots$.

Finally, the linear map \mathcal{W} implemented by one layer of the null MERA, and the proposed continuous metric $dl_{\mathcal{M}^p}^2$ for the geometry of the tensor network are

$$\mathcal{W} = 2^{iD}, \quad (261)$$

$$dl_{\mathcal{M}^p}^2 = a_{UV}^2 (x^2 ds^2 + 2x ds dx + dx^2). \quad (262)$$

We emphasize that, since a layer \mathcal{W} of null MERA does not implement either euclidean nor lorentzian time evolution, from a path integral perspective the geometry of the null MERA is neither the hyperbolic space H_2 nor the de Sitter spacetime dS_2 .

N. Discrete sequence of tensor network geometries (II)

To summarize, we have seen that the euclidean, lorentzian, and null MERA tensor networks on the line correspond to a discrete version of a CFT path integral over the hyperbolic plane H_2^p , the Poincare de Sitter spacetime dS_2^p , and light sheet L_2^p . Recall that these three geometries can be embedded in the same ambient space AdS_3^p , where both H_2^p and dS_2^p become L_2^p in the limit of a small radius $R \rightarrow 0$, see Figs. (13) and (14). We can similarly regard the null MERA \mathcal{M} on the line as a particular case of either the euclidean MERA \mathcal{M}_+ or lorentzian MERA \mathcal{M}_- on the line, namely when there are $q = 0$ transfer matrices \mathcal{T} or \mathcal{T}_- (implementing euclidean or real time evolution) between layers \mathcal{W} , see Fig. 19.

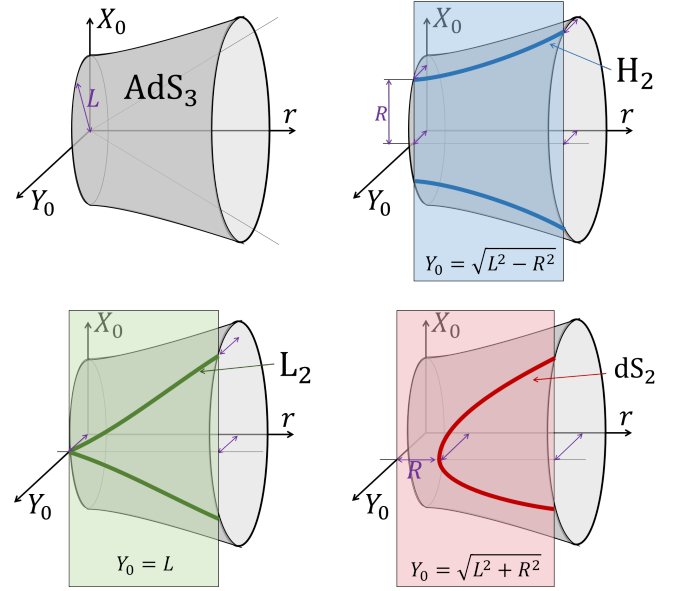


FIG. 20. Anti de Sitter spacetime AdS_3 with radius L , as embedded in Minkowski $\mathbb{R}^{2,2}$ with coordinates (X_0, Y_0, X_1, X_2) (notice that $r \equiv \sqrt{X_1^2 + X_2^2}$ is shown instead of X_1 and X_2 , so as to obtain a three dimensional projection of $\mathbb{R}^{2,2}$; each point should be augmented to a circle of radius r parameterized by $\theta \in [0, 2\pi)$). AdS_3 corresponds to the constraint $-X_0^2 - Y_0^2 + r^2 = -L^2$. The plot also shows H_2 , L_2 and dS_2 as the intersections of AdS_3 with hyperplanes defined by a constant value of Y_0 , namely $Y_0 = \sqrt{L^2 - R^2}$, $Y_0 = L$, and $Y_0 = \sqrt{L^2 + R^2}$, respectively. Each of these hyperplanes corresponds to a copy of Minkowski $\mathbb{R}^{1,2}$ as parameterized by (X_0, X_1, X_2) .

III. APPENDIX: EMBEDDING IN GLOBAL ANTI DE SITTER

In the context of the AdS/CFT correspondence, one may ask whether tensor networks such as MERA can be understood as a lattice realization of the holographic principle, in the sense of representing a two-dimensional slice of anti de Sitter spacetime AdS_3 [15–20].

The three two-dimensional geometries under consideration —hyperbolic plane H_2 (or hyperbolic disk), the light sheet L_2 (or light cone), and the de Sitter spacetime dS_2 — can also be embedded in AdS_3 , which in turn can be embedded in flat $\mathbb{R}^{2,2}$, as briefly reviewed below. Therefore, MERA and the proposed euclidean and lorentzian versions of MERA can be understood as discrete versions of 2d CFT path integrals on different types of 2d slices of AdS_3 .

Notice, however, that there is no additional, emergent, holographic dimension in a two-dimensional representation of a path integral of a two-dimensional CFT! Therefore it is unclear that the ability to embed the two-dimensional geometries H_2 , L_2 , and dS_2 attached to the above MERA tensor networks in AdS_3 should be interpreted as evidence that the tensor networks are a realization of holography.

Let X_0 and Y_0 denote time coordinates and X_1 and X_2 denote space coordinates, such that the metric of $\mathbb{R}^{2,2}$ reads

$$dl^2 = -dX_0^2 - dY_0^2 + dX_1^2 + dX_2^2. \quad (263)$$

Then AdS_3 is defined by the constraint

$$-X_0^2 - Y_0^2 + X_1^2 + X_2^2 = -L^2, \quad (264)$$

where L is the AdS radius, see Fig. 20.

Let us consider a parameterization of $\mathcal{R}^{2,2}$ in terms of new coordinates (L, t, r, θ) given by

$$X_0 = \sqrt{r^2 + L^2} \sin(t/L), \quad (265)$$

$$Y_0 = \sqrt{r^2 + L^2} \cos(t/L), \quad (266)$$

$$X_1 = r \cos(\theta), \quad (267)$$

$$X_2 = r \sin(\theta), \quad (268)$$

Notice that for any fixed value of L ,

$$-X_0^2 - Y_0^2 + X_1^2 + X_2^2 \quad (269)$$

$$= -(r^2 + L^2)(\cos^2 \theta + \sin^2 \theta) + r^2(\cos^2 \theta + \sin^2 \theta) \quad (270)$$

$$= -(r^2 + L^2) + r^2 = -L^2. \quad (271)$$

and thus this parameterization is consistent with the constraint (264) defining AdS_3 of radius L . The induced metric reads

$$dl^2 = -((r/L)^2 + 1) dt^2 + \frac{dr^2}{(r/L)^2 + 1} + r^2 d\theta^2. \quad (272)$$

As embedded in $\mathbb{R}^{2,2}$, the time direction t of AdS_3 is compact, namely $t/L \sim t/L + 2\pi$. By removing such identification, we then obtain a time coordinate t that can take any real value, $t \in (-\infty, \infty)$.

For visualization purposes, we also consider replacing the radial coordinate $r \in [0, \infty)$ in parameterization (265)-(268) with a new radial coordinate $\rho \in [0, \pi/2]$ given by

$$r/L = \tan(\rho), \quad (273)$$

in terms of which the metric becomes

$$dl^2 = \frac{1}{\cos^2 \rho} (-dt^2 + d\rho^2 + L^2 \sin^2 \rho d\theta^2). \quad (274)$$

This is the *soup can* representation of AdS_3 , see Fig. 21.

A. Family of \mathbf{H}_2 slices

Let us introduce an alternative parameterization of $\mathbb{R}^{2,2}$ in terms of coordinates (L, R, r, θ) given by:

$$X_0 = \sqrt{R^2 + r^2}, \quad (275)$$

$$Y_0 = \sqrt{L^2 - R^2}, \quad (276)$$

$$X_1 = r \cos(\theta), \quad (277)$$

$$X_2 = r \sin(\theta), \quad (278)$$

with $L \geq R > 0$, $r \geq 0$, $\theta \in [0, 2\pi)$. Notice that, again, a fixed value of L is still compatible with constraint (264) defining AdS_3 with radius L :

$$-X_0^2 - Y_0^2 + X_1^2 + X_2^2 \quad (279)$$

$$= -(R^2 + r^2) - (L^2 - R^2) + r^2(\cos^2 \theta + \sin^2 \theta) \quad (280)$$

$$= -L^2. \quad (281)$$

Then, for a fixed value of L and R (with $R < L$), we also notice the time coordinate Y_0 in Eq. (276) is just a constant and that the remaining coordinates (X_0, X_1, X_2) describe three-dimensional Minkowski spacetime $\mathbb{R}^{1,2}$ as in the previous section. Moreover, Eq. (275) can be interpreted as a constraint $X_0^2 = R^2 + r^2$ in $\mathbb{R}^{1,2}$, namely the constraint (37) defining \mathbf{H}_2 . Therefore, for each pair (L, R) with $R < L$, we have obtained a hyperbolic plane \mathbf{H}_2 with radius R , with metric (40), embedded in AdS_3 with radius L , see Fig. 20.

We can compare the two AdS_3 parameterizations (265)-(268) and (275)-(278) to conclude that

$$(r^2 + L^2) \cos^2(t/L) = L^2 - R^2 \quad (282)$$

or, in terms of the radial coordinate ρ ,

$$\cos(t/L) = \sqrt{1 - (R/L)^2} \cos \rho. \quad (283)$$

The corresponding surface is indicated in Fig. 21. Notice that for $R = L$ we obtain $\cos(t/L) = 0$, that is, the time slice $t = \pi/2$.

B. \mathbf{L}_2 slice

Let us introduce the parametrization

$$X_0 = \pm|r|, \quad (284)$$

$$Y_0 = L, \quad (285)$$

$$X_1 = r \cos(\theta), \quad (286)$$

$$X_2 = r \sin(\theta), \quad (287)$$

where we immediately recognize a three-dimensional manifold with coordinates (L, r, θ) embedded in $\mathbb{R}^{2,2}$ or, ignoring $Y_0 = L$ in Eq. (285), a two-dimensional manifold with coordinates (r, θ) embedded in $\mathbb{R}^{1,2}$, with (284) being equivalent to the constraint (33) defining the light cone \mathbf{L}_2 , see Fig. 20.

We can compare the two parameterizations (265)-(268) and (284) - (287) to conclude that

$$(r^2 + L^2) \cos^2(t/L) = L^2 \quad (288)$$

or, in terms of the radial coordinate ρ ,

$$\cos(t/L) = \cos \rho. \quad (289)$$

The corresponding surface is indicated in Fig. 21.

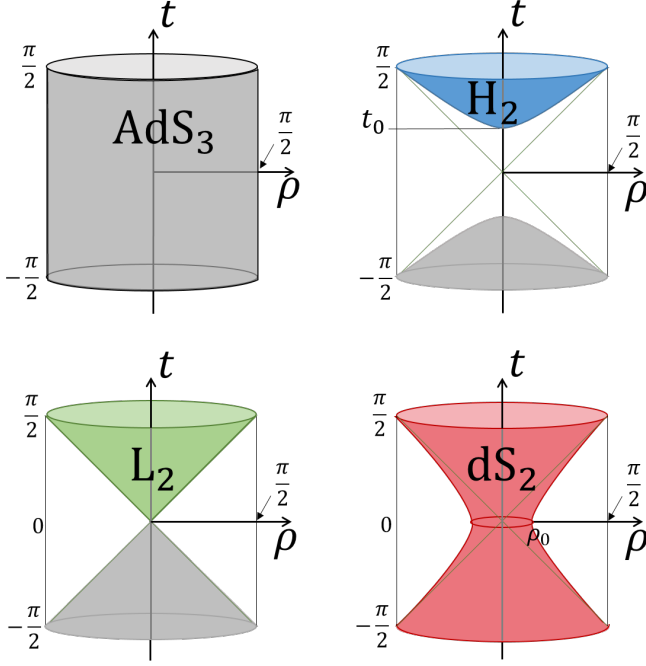


FIG. 21. AdS_3 in coordinates (t, ρ, θ) , where $t \in (-\infty, \infty)$ is the uncompactified time coordinate, $\rho \in [0, \pi/2)$ is a radial space coordinate, and $\theta \in [0, 2\pi)$ is an angular space coordinate. H_2 , L_2 , and dS_2 slices that hit the AdS_3 boundary $\rho = \pi/2$ at time $t = \pi/2$.

C. Family of dS_2 slices

We now introduce yet another parameterization of Minkowski $\mathbb{R}^{2,2}$ in terms of new coordinates (L, R, r, θ) this time given by

$$X_0 = \sqrt{r^2 - R^2}, \quad (290)$$

$$Y_0 = \sqrt{L^2 + R^2}, \quad (291)$$

$$X_1 = r \cos(\theta), \quad (292)$$

$$X_2 = r \sin(\theta), \quad (293)$$

where $r \geq R > 0$, $\theta \in [0, 2\pi)$. We can again check that a fixed value of L defines AdS_3 with radius $|L|$ (constraint (264)):

$$-X_0^2 - Y_0^2 + X_1^2 + X_2^2 \quad (294)$$

$$= -(r^2 - R^2) - (L^2 + R^2) + r^2 \cos^2 \theta + r^2 \sin^2 \theta \quad (295)$$

$$= -L^2. \quad (296)$$

Then, for a fixed value of L and R , we also notice the time coordinate Y_0 in Eq. (291) is just a constant and that the remaining coordinates (X_0, X_1, X_2) describe three-dimensional Minkowski spacetime $\mathbb{R}^{1,2}$ as in the previous section. Moreover, Eq. (290) can be interpreted as a constraint $X_0^2 = R^2 - r^2$ in $\mathbb{R}^{1,2}$, namely the constraint (38) defining dS_2 . Therefore, for each pair (L, R) we have obtained a hyperbolic plane H_2 with radius $|R|$ and metric (42), embedded in AdS_3 with radius $|L|$, see Fig. 20.

We can compare the two AdS_3 parameterizations (265)-(268) and (290)-(293) to conclude that

$$(r^2 + L^2) \cos^2(t/L) = L^2 + R^2 \quad (297)$$

or, in terms of the radial coordinate ρ ,

$$\cos(t/L) = \sqrt{1 + (R/L)^2} \cos \rho. \quad (298)$$

The corresponding surface is indicated in Fig. 21. Notice that for $R = \infty$ we obtain $\cos(\rho) = 0$, that is, the AdS_3 boundary $\rho = \pi/2$.

D. L_2 as the $R \rightarrow 0$ limit of H_2 , dS_2

Notice that the light cone geometry L_2 is recovered as the $R \rightarrow 0$ limit of both H_2 and dS_2 . Indeed, for $R = 0$, both the parametrization (275)-(278) of H_2 and the parametrization (290)-(293) of dS_2 coincide with the parametrization (284)-(287) of L_2 , and the relation (283) of H_2 and (298) of dS_2 agree with the relation (298) of dS_2 . See Fig. 6(c).

IV. GENERATOR OF THE LINEAR MAP OBTAINED THROUGH A PATH INTEGRAL

In this appendix we briefly review the parameterization of metric and the generator of linear map used in the appendices I and II above. These expressions have been justified in the Appendix of [47].

A. Euclidean

Consider the generic euclidean metric

$$g_{\mu\nu}(\tau, x) = \begin{pmatrix} g_{00}(\tau, x) & g_{01}(\tau, x) \\ g_{10}(\tau, x) & g_{11}(\tau, x) \end{pmatrix} \quad (299)$$

$$= \Omega^2(\tau, x) \begin{pmatrix} a(\tau, x)^2 + b(\tau, x)^2 & b(\tau, x) \\ b(\tau, x) & 1 \end{pmatrix} \quad (300)$$

Then the path integral on a thin strip with boundaries Σ and Σ' at $\tau = \tau_0$ and $\tau = \tau_0 + \epsilon$ produces a linear map $V : \mathcal{H}_\Sigma \rightarrow \mathcal{H}_{\Sigma'}$ between the QFT Hilbert spaces \mathcal{H}_Σ and $\mathcal{H}_{\Sigma'}$ at Σ and Σ' . When point $(\tau_0, x) \in \Sigma$ is identified with point $(\tau_0 + \epsilon, x) \in \Sigma'$, then the two Hilbert spaces \mathcal{H}_Σ and $\mathcal{H}_{\Sigma'}$ can be identified accordingly and we refer to them simply as \mathcal{H} . The linear map $V : \mathcal{H} \rightarrow \mathcal{H}$ for small ϵ reads

$$V \approx \mathbb{1} - \epsilon(Q_0 - iQ_1) \quad (301)$$

where

$$Q_0 \equiv \int_\Sigma dx \, a(\tau, x) \, h_L(\tau, x), \quad (302)$$

$$Q_1 \equiv \int_\Sigma dx \, b(\tau, x) \, p_L(\tau, x), \quad (303)$$

and where h_L and p_L are the Lorentzian Hamiltonian and momentum densities *in flat spacetime*. For instance, for the free boson they read

$$h_L \equiv \frac{1}{2} ((\partial_t \phi)^2 + (\partial_x \phi)^2), \quad (304)$$

$$p_L \equiv -\partial_t \phi \partial_x \phi. \quad (305)$$

Specializing to $a(\tau, x) = a$ and $b(\tau, x) = b$ we have

$$Q_0 = a \int_{\Sigma} dx h_L \equiv a H, \quad (\text{Hamiltonian operator}) \quad (306)$$

$$Q_1 = b \int_{\Sigma} dx p_L \equiv b P, \quad (\text{momentum operator}) \quad (307)$$

and a finite map reads

$$V = \exp(-aH + ibP), \quad (308)$$

as we expected. Moreover, for $a = 0$ and $b(\tau, x) = \alpha x$ we have

$$Q_0 = 0, \quad (309)$$

$$Q_1 = b \int_{\Sigma} dx x p_L \equiv \alpha D \quad (\text{dilation operator}) \quad (310)$$

and a finite map reads

$$V = \exp(i\alpha D). \quad (311)$$

B. Lorentzian

Consider now the generic lorentzian metric

$$g_{\mu\nu}(\tau, x) = \begin{pmatrix} g_{00}(t, x) & g_{01}(t, x) \\ g_{10}(t, x) & g_{11}(t, x) \end{pmatrix} \quad (312)$$

$$= \Omega^2(t, x) \begin{pmatrix} -a(t, x)^2 + b(t, x)^2 & b(t, x) \\ b(t, x) & 1 \end{pmatrix} \quad (313)$$

Then the path integral on a thin strip with boundaries Σ and Σ' at $t = t_0$ and $t = t_0 + \epsilon$ produces a linear map $V : \mathcal{H}_{\Sigma} \rightarrow \mathcal{H}_{\Sigma'}$ between the QFT Hilbert spaces \mathcal{H}_{Σ} and $\mathcal{H}_{\Sigma'}$ at Σ and Σ' . When point $(t_0, x) \in \Sigma$ is identified with point $(t_0 + \epsilon, x) \in \Sigma'$, then the two Hilbert spaces \mathcal{H}_{Σ} and $\mathcal{H}_{\Sigma'}$ can again be identified accordingly and we refer to them simply as \mathcal{H} . The linear map $V : \mathcal{H} \rightarrow \mathcal{H}$ for small ϵ now reads

$$V \approx \mathbb{1} - i\epsilon Q_0 + i\epsilon Q_1 \quad (314)$$

where Q_0 and Q_1 are as defined above in the euclidean case.

Specializing to $a(\tau, x) = a$ and $b(\tau, x) = b$ the finite map reads

$$V = \exp(-iaH + ibP), \quad (315)$$

as we expected. For $a = 0$ and $b(\tau, x) = \alpha x$ we again have

$$V = \exp(i\alpha D). \quad (316)$$

Notice that the generator Q_1 appears identically in both the euclidean and lorentzian cases, that is $V \approx \mathbb{1} + iQ_1$, whereas the generator Q_0 appears as

$$V_E \approx \mathbb{1} - \epsilon Q_0, \quad V_L \approx \mathbb{1} - i\epsilon Q_0, \quad (317)$$

which is consistent with

$$V_E = \exp(-\tau H), \quad V_L = \exp(-itH), \quad (318)$$

for the case of Hamiltonian evolution under the relation $\tau = it$, as expected.

V. APPENDIX: LOW ENERGY IDENTIFICATION BETWEEN SPIN CHAINS OF DIFFERENT SIZE

A layer \mathcal{W} of optimized MERA defines a linear map (also denoted by \mathcal{W}) between the Hilbert spaces of two periodic spin chains, one of size N (bottom chain) and the other of size $N/2$ (top chain). We would like to characterize this linear map \mathcal{W} as a discrete version of a linear map V acting on the Hilbert space of a CFT on the circle, as a means to relate the layer \mathcal{W} to a CFT path integral on a strip geometry compatible with the linear map V .

Fortunately, we can use the techniques of Refs. [50–52], which are based on work by Cardy [48] and by Koo and Saleur [49], to relate a basis of *low energy* states $\{|\phi_{\alpha}^N\rangle\}$ and $\{|\phi_{\alpha}^{N/2}\rangle\}$ on each of the two spin chains with CFT states $|\phi_{\alpha}^{\text{CFT}}\rangle$, so that the matrix elements $\langle\phi_{\beta}^{N/2}|\mathcal{W}|\phi_{\alpha}^N\rangle$ can be directly compared to the corresponding matrix elements $\langle\phi_{\beta}^{\text{CFT}}|V|\phi_{\alpha}^{\text{CFT}}\rangle$ on the CFT. Below we explain how this is accomplished, step by step. Importantly, the three conjectured possible forms of V , namely

$$V = \begin{cases} e^{-\frac{R}{r}H} = \sum_{\alpha} e^{-\frac{R}{r}E_{\alpha}} |\phi_{\alpha}^{\text{CFT}}\rangle \langle\phi_{\alpha}^{\text{CFT}}| & (\text{H}_2) \\ e^0 = \sum_{\alpha} |\phi_{\alpha}^{\text{CFT}}\rangle \langle\phi_{\alpha}^{\text{CFT}}| & (\text{L}_2) \\ e^{-i\frac{R}{r}H} = \sum_{\alpha} e^{-i\frac{R}{r}E_{\alpha}} |\phi_{\alpha}^{\text{CFT}}\rangle \langle\phi_{\alpha}^{\text{CFT}}| & (\text{dS}_2) \end{cases} \quad (319)$$

are all diagonal in the basis $|\phi_{\alpha}^{\text{CFT}}\rangle$ of simultaneous eigenvectors of the Hamiltonian and momentum operators. In particular, in order to distinguish between the last two options, which only differ by complex phases, special care is needed to properly fix the arbitrary complex phase of each state $|\phi_{\alpha}^N\rangle$ and $|\phi_{\alpha}^{N/2}\rangle$ (which unavoidably appears as a result of the diagonalization of the Hamiltonian and momentum operators on N and $N/2$ sites).

A. Operator-state correspondence

The operator-state correspondence of conformal field theory [55–57] implies that the scaling operators $\phi_{\alpha}^{\text{CFT}}(x)$ of a given CFT are in one-to-one correspondence with the states $|\phi_{\alpha}^{\text{CFT}}\rangle$ of the Hilbert space of that CFT on the circle.

Let Δ_α and S_α be the scaling dimension and conformal spin of the scaling operator ϕ_α^{CFT} and let E_α^{CFT} and P_α^{CFT} be the energy and momentum of a simultaneous eigenstate $|\phi_\alpha^{\text{CFT}}\rangle$ of the Hamiltonian operator H^{CFT} and momentum operator P^{CFT}

$$H^{\text{CFT}} \equiv \int_0^L dx h(x), \quad P^{\text{CFT}} \equiv \int_0^L dx p(x), \quad (320)$$

on a circle of length L , where $h(x)$ and $p(x)$ are the hamiltonian and momentum densities of the CFT. Then a first consequence of the operator-state correspondence is that

$$E_\alpha^{\text{CFT}} = \frac{2\pi}{L} \left(\Delta_\alpha - \frac{c}{12} \right), \quad P_\alpha^{\text{CFT}} = \frac{2\pi}{L} S_\alpha. \quad (321)$$

The above spectral relations are sometimes already sufficient in order to identify the state $|\phi_\alpha^{\text{CFT}}\rangle$ with the corresponding operator ϕ_α^{CFT} . However, the spectra of energies and momenta (equivalently, of scaling dimensions and conformal spins) generically contains degeneracies, that is, there are pairs $(E_\alpha^{\text{CFT}}, P_\alpha^{\text{CFT}}) = (E_{\alpha'}^{\text{CFT}}, P_{\alpha'}^{\text{CFT}})$ for $\alpha \neq \alpha'$. In order to correctly identify each state with its corresponding operator we can then use that the states $|\phi_\alpha^{\text{CFT}}\rangle$ are organized in irreducible representations of the conformal group, or conformal towers, with Virasoro generators given by

$$L_n^{\text{CFT}} \equiv \frac{L}{(2\pi)^2} \int_0^L dx e^{+inx \frac{2\pi}{L}} T(x) + \frac{c}{24} \delta_{n,0}, \quad (322)$$

$$\bar{L}_n^{\text{CFT}} \equiv \frac{L}{(2\pi)^2} \int_0^L dx e^{-inx \frac{2\pi}{L}} \bar{T}(x) + \frac{c}{24} \delta_{n,0}, \quad (323)$$

where $T(x)$ and $\bar{T}(x)$ are the holomorphic and antiholomorphic components of the stress tensor,

$$T(x) \equiv 2\pi \frac{h(x) + p(x)}{2}, \quad \bar{T}(x) \equiv 2\pi \frac{h(x) - p(x)}{2}, \quad (324)$$

or $h(x) = (T(x) + \bar{T}(x))/2\pi$ and $p(x) = (T(x) - \bar{T}(x))/2\pi$, and c is the central charge of the CFT. For example, the ground state/identity state $|\mathbb{1}^{\text{CFT}}\rangle$ relates to the stress tensor states $|T^{\text{CFT}}\rangle$ and $|\bar{T}^{\text{CFT}}\rangle$ through

$$L_{-2}^{\text{CFT}} |\mathbb{1}^{\text{CFT}}\rangle = \sqrt{\frac{c}{2}} |T^{\text{CFT}}\rangle, \quad \bar{L}_{-2}^{\text{CFT}} |\mathbb{1}^{\text{CFT}}\rangle = \sqrt{\frac{c}{2}} |\bar{T}^{\text{CFT}}\rangle. \quad (325)$$

Thus we can use this expression in order to unambiguously identify states $|T^{\text{CFT}}\rangle$ and $|\bar{T}^{\text{CFT}}\rangle$ in the list $\{|\phi_\alpha^{\text{CFT}}\rangle\}$ of simultaneous eigenstates of H^{CFT} and P^{CFT} and, importantly for our purposes, remove any spurious relative complex phase between states $|\mathbb{1}^{\text{CFT}}\rangle$, $|T^{\text{CFT}}\rangle$, and $|\bar{T}^{\text{CFT}}\rangle$. Indeed, notice that if $e^{i\varphi}$ is a random complex phase, both $|T^{\text{CFT}}\rangle$ and $e^{i\varphi}|T^{\text{CFT}}\rangle$ are equally valid simultaneous eigenvectors of H^{CFT} and P^{CFT} , but only the choice $e^{i\varphi} = 1$ is compatible with Eq. (325). Thus we can use Eq. (325) to set the relative complex phase $e^{i\varphi}$ between $|\mathbb{1}^{\text{CFT}}\rangle$ and $|T^{\text{CFT}}\rangle$ to 1 (and similarly for the relative complex phase between $|\mathbb{1}^{\text{CFT}}\rangle$ and $|\bar{T}^{\text{CFT}}\rangle$). More generally, any descendant state $|\phi_\alpha^{\text{CFT}}\rangle$ in the conformal

tower of the ground state/identity primary state $|\mathbb{1}^{\text{CFT}}\rangle$ is equal to some known linear combination of strings of operators L_n 's and \bar{L}_n 's acting on $|\mathbb{1}^{\text{CFT}}\rangle$, which we can use to unambiguously identify the descendant state and remove any spurious relative complex phase within this conformal tower.

Moreover, given any other primary operator χ^{CFT} , the Virasoro generators L_n and \bar{L}_n similarly connect the corresponding primary state $|\chi^{\text{CFT}}\rangle$ with all its descendant states $|\phi_\alpha^{\text{CFT}}\rangle$, which leads to their unambiguous identification with operators ϕ_α^{CFT} and the removal of spurious relative complex phases within the conformal tower. For instance, for the Ising CFT, this allow us to identify each state $|\phi_\alpha^{\text{CFT}}\rangle$ as a concrete descendant of one of its three primary states: the identity primary state $|\mathbb{1}^{\text{CFT}}\rangle$, the spin primary state $|\sigma^{\text{CFT}}\rangle$ and the energy density primary state $|\epsilon^{\text{CFT}}\rangle$. Moreover, any spurious relative complex phase within each of the conformal towers has been removed.

The generators of the conformal group, the Virasoro generators L_n and \bar{L}_n connect states within each conformal tower and that allowed us to unambiguously identify each state $|\phi_\alpha^{\text{CFT}}\rangle$ with its corresponding scaling operators ϕ_α^{CFT} as well as to eliminate a spurious complex phase (introduced during the diagonalization of H^{CFT} and P^{CFT}) within each conformal tower. However, we are left with a spurious complex phase relative of any conformal tower with respect to the identity tower. Given a primary operator χ^{CFT} , we can remove the remaining spurious complex phase $e^{i\phi_\chi}$ between the ground state $|\mathbb{1}^{\text{CFT}}\rangle$ (and its descendant states) and the primary state $|\chi^{\text{CFT}}\rangle$ (and its descendant states) using known CFT matrix elements such as [52]

$$\langle \chi^{\text{CFT}} | \chi^{\text{CFT},0} | \mathbb{1}^{\text{CFT}} \rangle = \left(\frac{2\pi}{L} \right)^{\Delta_\chi}, \quad (326)$$

where we assumed for simplicity that χ^{CFT} has conformal spin $S_\alpha = 0$, and where

$$\chi_\alpha^{\text{CFT},0} \equiv \frac{1}{L} \int_0^L dx \chi_\alpha^{\text{CFT}}(x) \quad (327)$$

is the zero Fourier mode of the primary operator χ_α^{CFT} . In this way, all complex phases between all the states in the CFT have been fixed, and we are only left with a global complex phase.

B. H_n^{CFT} instead of L_n^{CFT}

For later reference, we point out that the relations in the example of Eq. (325) are equivalent to the less standard expressions

$$H_{-2}^{\text{CFT}} |\mathbb{1}^{\text{CFT}}\rangle = \sqrt{\frac{c}{2}} |T^{\text{CFT}}\rangle, \quad H_2^{\text{CFT}} |\mathbb{1}^{\text{CFT}}\rangle = \sqrt{\frac{c}{2}} |\bar{T}^{\text{CFT}}\rangle, \quad (328)$$

in terms of the Fourier mode H_n^{CFT} of the Hamiltonian density $h(x)$,

$$H_n^{\text{CFT}} \equiv \frac{L}{2\pi} \int_0^L dx e^{inx \frac{2\pi}{L}} h(x) \quad (329)$$

$$= L_n + \bar{L}_{-n} - \frac{c}{12} \delta_{n,0}, \quad (330)$$

where we note that

$$H_0^{\text{CFT}} = L_0^{\text{CFT}} + \bar{L}_0^{\text{CFT}} - \frac{c}{12} = \frac{L}{2\pi} H^{\text{CFT}}. \quad (331)$$

More generally, the identification of states $|\phi_\alpha^{\text{CFT}}\rangle$ with their corresponding operators ϕ_α^{CFT} and the removal of spurious relative complex phases within a conformal tower can be conducted using the Fourier modes H_n^{CFT} of the Hamiltonian density $h(x)$ instead of the Fourier modes L_n and \bar{L}_n of the stress tensor components $T(x)$ and $\bar{T}(x)$.

Here we notice that although H_n^{CFT} in Eq. (334) acts as a concrete linear combination of the two Virasoro generators L_n^{CFT} and $\bar{L}_{-n}^{\text{CFT}}$, we can always split the result of acting with H_n^{CFT} on a given energy/momentum eigenstate $|\phi_\alpha^{\text{CFT}}\rangle$ into *higher energy* and *lower energy* contributions, which for $n < 0$ will correspond to having acted on $|\phi_\alpha^{\text{CFT}}\rangle$ with L_n and \bar{L}_{-n} , respectively (and for $n > 0$ will correspond to having acted on $|\phi_\alpha^{\text{CFT}}\rangle$ with \bar{L}_{-n} and L_n , respectively). Indeed, both L_n and \bar{L}_n lower the energy (by $n2\pi/L$) for $n > 0$ and increase the energy (by $n2\pi/L$) for $n < 0$.

C. One spin chain

All the above manipulations referred to the CFT in the continuum. On the lattice, we can also identify each simultaneous eigenstate $|\phi_\alpha\rangle$ of a critical quantum spin chain Hamiltonian $H = \sum_{j=1}^N h_j$ and one-site translation $T = e^{-iP}$ operators,

$$H|\phi_\alpha\rangle = E_\alpha|\phi_\alpha\rangle, \quad T|\phi_\alpha\rangle = e^{-iP_\alpha}|\phi_\alpha\rangle, \quad (332)$$

with its corresponding CFT scaling operators ϕ_α^{CFT} , and eliminate spurious complex phases, as we did in the continuum. For that purpose we will use *approximate* lattice versions of several continuum expressions mentioned above. First, as pointed out by Cardy [48], on the lattice the low energy spectra of energies and momenta resemble the CFT result (321) by replacing the length L of the circle with the number of sites N in the periodic quantum spin chain,

$$E_\alpha \approx \frac{2\pi}{N} \left(\Delta_\alpha - \frac{c}{12} \right), \quad P_\alpha = \frac{2\pi}{N} S_\alpha. \quad (333)$$

Here \approx indicates that we are neglecting non-universal sub-leading contributions which typically scale as $O(N^{-1-\gamma})$ for some $\gamma > 0$. In some cases, this already allows us to relate a lattice state $|\phi_\alpha\rangle$ with its corresponding scaling operator ϕ_α^{CFT} . More generally, however, we

need to resort to the Koo-Saleur formula [49], which provides a lattice version of the Virasoro generators L_n^{CFT} and \bar{L}_n^{CFT} in Eqs. (322)-(323) or, following Refs. [50, 51], the equivalent but more convenient lattice version H_n of the Fourier modes H_n^{CFT} of the Hamiltonian density in Eq. (329), namely

$$H_n \equiv \frac{N}{2\pi} \sum_{j=1}^N e^{+inj \frac{2\pi}{N}} h_j, \quad H_0 = \frac{N}{2\pi} H. \quad (334)$$

We can use this lattice Fourier modes H_n similarly as in the continuum. For instance, the approximate lattice version of Eq. (328) is

$$H_{-2}|\mathbb{1}\rangle \approx \sqrt{\frac{c}{2}}|T\rangle, \quad H_2|\mathbb{1}\rangle \approx \sqrt{\frac{c}{2}}|\bar{T}\rangle, \quad (335)$$

which we can use to unambiguously identify the lattice states $|T\rangle$ and $|\bar{T}\rangle$ by acting on the ground state $|\mathbb{1}\rangle$, while at the same time removing any spurious complex phase between these states. In this way we are only left with a spurious complex phase $e^{i\varphi_\chi}$ between the identity tower and the tower of each other primary state $|\chi\rangle$. The next step is to follow Ref. [52] in order to identify a lattice version χ_j (acting around site j) of each CFT primary operator $\chi^{\text{CFT}}(x)$, then build its zero Fourier mode

$$\chi^0 \equiv \frac{1}{N} \sum_{j=1}^N \chi_j, \quad (336)$$

where again for simplicity we assumed $S_\chi = 0$, and then use the approximate, lattice version of Eq. (326),

$$\langle \chi | \chi^0 | \mathbb{1} \rangle \approx \left(\frac{2\pi}{L} \right)^{\Delta_\chi}, \quad (337)$$

to remove the complex phase $e^{i\varphi_\chi}$. For instance, for the Ising model, the lattice version of the spin primary operator $\sigma^{\text{CFT}}(x)$ and of the energy density primary operator $\epsilon^{\text{CFT}}(x)$ are, approximately, given by [52]

$$\sigma_j \approx \sigma_j^x, \quad \epsilon_{j+1/2} \approx \sigma_j^x \sigma_{j+1}^x - (\sigma_j^z + \sigma_{j+1}^z)/2, \quad (338)$$

and we eliminate spurious complex phases $e^{i\varphi_\sigma}$ and $e^{i\varphi_\epsilon}$ by requiring that the matrix elements $\langle \sigma | \sigma^0 | \mathbb{1} \rangle$ and $\langle \epsilon | \epsilon^0 | \mathbb{1} \rangle$ are approximately as expected in the CFT, namely

$$\langle \sigma | \sigma^0 | \mathbb{1} \rangle = \left(\frac{2\pi}{L} \right)^{1/8}, \quad \langle \epsilon | \epsilon^0 | \mathbb{1} \rangle = \left(\frac{2\pi}{L} \right)^1. \quad (339)$$

D. Two spin chains

Finally, let us consider two spin chains of size N and $N/2$. Using the lattice Fourier modes H_n on each chain, we can identify simultaneous eigenstates $|\phi_\alpha^N\rangle$ of H and

P on N sites with simultaneous eigenstates $|\phi_\alpha^{N/2}\rangle$ of H and P on $N/2$ sites

$$|\phi_\alpha^N\rangle \sim |\phi_\alpha^{N/2}\rangle. \quad (340)$$

through the identifications $|\phi_\alpha^N\rangle \sim |\phi_\alpha^{\text{CFT}}\rangle$ and $|\phi_\alpha^{N/2}\rangle \sim |\phi_\alpha^{\text{CFT}}\rangle$. We can also use H_n and the matrix elements of the type (337) to eliminate all relative complex phases within the low energy states of N sites and of $N/2$ sites separately. Then there is still one relative complex phase $e^{i\varphi^{N \rightarrow N/2}}$ (independent of α and β) that affects our identification of states $|\phi_\alpha^N\rangle$ on N spins with states $|\phi_\alpha^{N/2}\rangle$ of $N/2$ spins. As a result, the matrix element

$$\mathcal{W}_{\alpha\beta} \equiv \langle \phi_\alpha^N | \mathcal{W} | \phi_\beta^{2N} \rangle \quad (341)$$

is proportional to this arbitrary complex phase $e^{i\varphi^{N \rightarrow N/2}}$, which we eliminate by demanding that $\mathcal{W}_{11} =$

$\langle 1^{N/2} | \mathcal{W} | 1^N \rangle$ be positive.

A numerical exploration then shows that, after a consistent choice of reference frame across different spin chains (see below), the linear map \mathcal{W} acts on low energy states as the identity map,

$$\mathcal{W}_{\alpha\beta} \approx \delta_{\alpha\beta}. \quad (342)$$

Specifically, Table I shows the order of magnitude of $|\mathcal{W}_{\alpha\beta} - \delta_{\alpha\beta}|$ for the 17 lowest energy eigestates of a coarse-grained version of the Ising model, when \mathcal{W} connects the low energy states of a spin chain with $N = 8$ sites to low energy states of a spin chain with $N/2 = 4$ sites. Here, each site is described by a vector space of dimension $\chi = 8$ and effectively represents dozens of spins of the original Ising model.

	I	σ	ε	$\partial\sigma$	$\bar{\partial}\sigma$	T	$\partial\varepsilon$	$\bar{\partial}\varepsilon$	\bar{T}	$\partial\bar{\partial}\sigma$	$\partial^2\sigma$	$\bar{\partial}^2\sigma$	$\partial\bar{\partial}\varepsilon$	∂T	$\partial^2\varepsilon$	$\bar{\partial}^2\varepsilon$	$\bar{\partial}T$
I	10^{-5}	0	10^{-2}	0	0	0	0	0	0	0	0	0	10^{-3}	0	0	0	0
σ	0	10^{-5}	0	0	0	0	0	0	0	10^{-3}	0	0	0	0	0	0	0
ε	10^{-2}	0	10^{-5}	0	0	0	0	0	0	0	0	0	10^{-5}	0	0	0	0
$\partial\sigma$	0	0	0	10^{-5}	0	0	0	0	0	0	0	0	0	0	0	0	0
$\bar{\partial}\sigma$	0	0	0	0	10^{-5}	0	0	0	0	0	0	0	0	0	0	0	0
T	0	0	0	0	0	10^{-4}	0	0	0	0	0	0	0	0	0	10^{-3}	0
$\partial\varepsilon$	0	0	0	0	0	0	10^{-4}	0	0	0	0	0	0	0	0	0	10^{-3}
$\bar{\partial}\varepsilon$	0	0	0	0	0	0	0	10^{-4}	0	0	0	0	0	10^{-3}	0	0	0
\bar{T}	0	0	0	0	0	0	0	0	10^{-4}	0	0	0	0	0	10^{-3}	0	0
$\partial\bar{\partial}\sigma$	0	10^{-3}	0	0	0	0	0	0	0	10^{-5}	0	0	0	0	0	0	0
$\partial^2\sigma$	0	0	0	0	0	0	0	0	0	0	10^{-3}	10^{-3}	0	0	0	0	0
$\bar{\partial}^2\sigma$	0	0	0	0	0	0	0	0	0	0	0	10^{-3}	0	0	0	0	0
$\partial\bar{\partial}\varepsilon$	10^{-3}	0	10^{-5}	0	0	0	0	0	0	0	0	0	10^{-4}	0	0	0	0
∂T	0	0	0	0	0	0	0	10^{-3}	0	0	0	0	0	10^{-3}	0	0	0
$\partial^2\varepsilon$	0	0	0	0	0	0	0	0	10^{-3}	0	0	0	0	0	10^{-3}	0	0
$\bar{\partial}^2\varepsilon$	0	0	0	0	0	10^{-3}	0	0	0	0	0	0	0	0	0	10^{-3}	0
$\bar{\partial}T$	0	0	0	0	0	0	10^{-3}	0	0	0	0	0	0	0	0	0	10^{-3}

TABLE I. Order of magnitude of matrix elements of $V - I$, labelled by CFT operators. Matrix elements $\leq 10^{-10}$ are shown as “0”. The asymmetry in the $\partial^2\sigma, \bar{\partial}^2\sigma$ sector is due to using one of these matrix elements to break a momentum degeneracy in the coarse system.

E. Consistent reference frame across spin chains

In order to characterize the action of one layer \mathcal{W} of optimized MERA as a map between the low energy subspaces of two critical quantum spin chain of sizes N and $N/2$, eventually resulting in (342) above, we made a convenient choice of the origin of the angle θ measuring the position of the spins in the chains. For a spin chain of size

$N = 2^T$ for some integer $T > 2$, we chose the position of the spins to be at angles

$$\theta_j^{(N)} = \frac{2\pi}{N} \left(j + \frac{1}{2} \right), \quad (343)$$

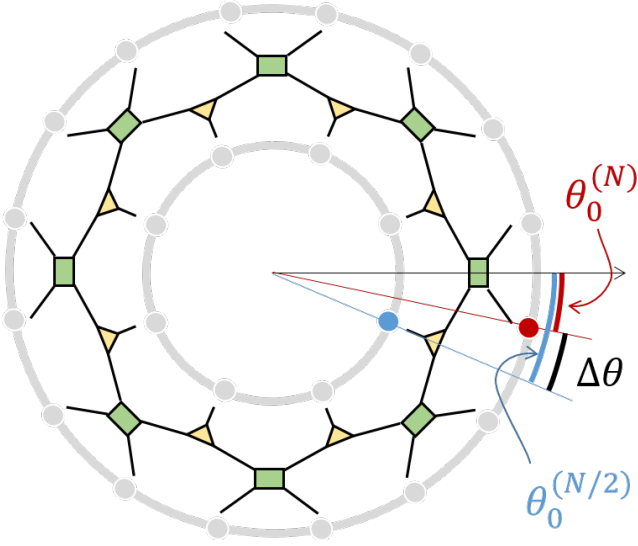


FIG. 22. The difference $\Delta\theta$ in the reference angles θ_N and $\theta_{N/2}$ for the N spin and the $N/2$ spin chains is of $1/2 \times 2\pi/N$ (half of a one-site translation in the N spin chain).

see Figs. (2) and (22), so that the Hamiltonian Fourier modes H_n are not actually taken as in Eq. (334) but as

$$H_n^{(N)} \equiv \frac{N}{2\pi} \sum_{j=1}^N e^{+in\theta_j^{(N)}} h_j \quad (344)$$

$$= \frac{N}{2\pi} \sum_{j=1}^N e^{+in(j+\frac{1}{2})\frac{2\pi}{N}} h_j. \quad (345)$$

The reason for this choice, which places the origin $\theta = 0$ half way between two lattice sites, is that it can be chosen consistently for chains of size N and $N/2$. Indeed, had we chosen $H_n^{(N)} = \frac{N}{2\pi} \sum_{j=1}^N e^{+inj\frac{2\pi}{N}} h_j$, and thus $H_n^{(N/2)} = \frac{N}{4\pi} \sum_{j=1}^{N/2} e^{+inj\frac{4\pi}{N}} h_j$, which amounts to considering that the $j = 0$ sites is at angle 0 for both spin chains, then we would observe that \mathcal{W} effectively implements a rotation by angle $\Delta\theta \equiv 1/2 \times 2\pi/N$ in mapping the spin chain of size N to the spin chain of size $N/2$, in such a way that its matrix elements now would be

$$\mathcal{W}_{\alpha\beta} \approx \delta_{\alpha\beta} e^{i\Delta\theta S_\alpha}, \quad (346)$$

where S_α is the conformal spin of state $|\phi_\alpha^N\rangle$.

To summarize, if we choose a consistent reference frame for θ across spin chains of different sizes, then the layer \mathcal{W} of optimized MERA is seen to act as the identity map between low energy subspaces. If, instead, in going from one spin chain to another one we implicitly apply a translation by an angle $\Delta\theta$ (by changing the reference frame), then the same layer \mathcal{W} of optimized MERA implements this translation by an angle $\Delta\theta$. Importantly, in none of these cases, the linear map \mathcal{W} adds a Boltzmann weight $e^{-\mu E_\alpha}$ or a complex phase $e^{-i\mu E_\alpha}$ to state $|\phi_\alpha\rangle$ (for any measurable $\mu > 0$), as it would happen in an euclidean or lorentzian path integral.